NASA TN D-1047

TECHNICAL NOTE

D-1047

RECOVERY TEMPERATURE, TRANSITION, AND HEAT-TRANSFER MEASUREMENTS AT MACH 5

By Paul F. Brinich

Lewis Research Center
Cleveland, Ohio

NATIONAL AERONAUTICS AND SPACE ADMINISTRATION
WASHINGTON
August 1961

NATIONAL AERONAUTICS AND SPACE ADMINISTRATION

TECHNICAL NOTE D-1047

RECOVERY TEMPERATURE, TRANSITION, AND HEAT-TRANSFER MEASUREMENTS AT MACH 5

By Paul F. Brinich

SUMMARY

Schlieren, recovery temperature, and heat-transfer measurements were made on a hollow cylinder and a cone with axes alined parallel to the stream. Both the cone and cylinder were equipped with various bluntnesses, and the tests covered a Reynolds number range up to 20×10^6 at a free-stream Mach number of 4.95 and wall to free-stream temperature ratios from 1.8 to 5.2 (adiabatic).

A substantial transition delay due to bluntness was found for both the cylinder and the cone. For the present tests (Mach 4.95), transition was delayed by a factor of 3 on the cylinder and about 2 on the cone, these delays being somewhat larger than those observed in earlier tests at Mach 3.1. Heat-transfer tests on the cylinder showed only slight effects of wall temperature level on transition location; this is to be contrasted to the large transition delays observed on conical-type bodies at low surface temperatures at Mach 3.1.

The schlieren and the peak-recovery-temperature methods of detecting transition were compared with the heat-transfer results. The comparison showed that the first two methods identified a transition point which occurred just beyond the end of the laminar run as seen in the heat-transfer data.

INTRODUCTION

The striking effect of leading-edge or tip bluntness of an aerodynamic body on the downstream movement of the transition point, and the consequent reductions in heat transfer noted in the wind tunnel tests of references 1 to 4 at Mach 3.1, have made an extension of these investigations to higher Mach numbers of considerable interest. The intent of the present investigation was to repeat certain of the tests

made at Mach 3.1, but at a higher Mach number of 5, and to utilize the same test facilities insofar as possible in order to establish dependable correlations with the earlier data.

References 1 and 3 presented the first systematic investigation of the effect of bluntness on the location of the transition point and on the equilibrium recovery temperature distribution at supersonic speeds. Briefly, it was found that for a two-dimensional boundary layer in an essentially zero pressure gradient both the transition point and the surface recovery temperature were extremely sensitive to minute changes in the sharpness of the body leading edge. For example, it was found that an increase in leading-edge thickness from 0.001 to 0.005 inch could easily double the length of the laminar run at Mach 3.1. This effect, together with a general increase in recovery temperature level, could be qualitatively accounted for by the existence of a shock-produced shear layer at the surface, as explained in reference 2.

The situation on a conical body, however, was not so amenable to treatment, for the location of the transition point was not nearly as sensitive to tip blunting as was the two-dimensional body. A part of this result is to be expected since, for the cone, bluntness exists essentially at a point, whereas a two-dimensional body has the bluntness distributed over the length of the leading edge. Notwithstanding this effect, which is accounted for in reference 2, the blunted conical body showed far less effect of tip blunting than did the two-dimensional body. No satisfactory explanation for this behavior has been proposed.

Up to this point, the experiments discussed have been conducted without heat transfer. In the presence of heat transfer to a precooled conical-type body, however, it was found in reference 4 that large delays in transition were possible by blunting the cone tip and that these delays were comparable to those anticipated in reference 2. No reasonable explanation for the different magnitudes of the transition delay on a blunted cone with and without heat transfer has been proposed.

In view of these interesting but inconclusive results, it was decided to continue the investigation at a Mach number of 5. A brief review of other high Mach number tests indicated that the transition Reynolds numbers increased substantially with increases in Mach number. This would cause the transition point on the conical body tested in reference 4 to move farther downstream, which meant that it probably would move off the model surface. Further practical design considerations precluded use of a larger cone model with the increasingly cumbersome auxiliary cooling equipment. As a result of these considerations, it was decided to construct a cylinder model similar to the one used in references 1 and 3, but which provided for precooling and could be inserted in the wind tunnel satisfactorily.

The results to be presented in this paper therefore include transition, recovery factor distribution, and heat transfer on a hollow cylindrical body alined with the airstream. The parameters that were varied, as in references 1, 3, and 4, were the unit Reynolds number (stagnation pressure variation) and the leading-edge bluntness. To extend the cone work done in reference 3, a 5°-included-angle cone equipped with various tip bluntnesses was used, but in the condition of zero heat transfer only. These tests were conducted in the Lewis 1- by 1-foot variable Reynolds number wind tunnel at a nominal Mach number of 5, during the interval June 1958 to March 1959.

E-797

APPARATUS, INSTRUMENTATION, AND PROCEDURE

The two models used in this investigation were a hollow cylinder and a 5°-included-angle cone. These models were placed in the 1- by 1-foot variable Reynolds number wind tunnel with their centerlines alined parallel to the tunnel centerline. Both models were tested over a Reynolds number range and with varying degrees of bluntness. Their installation in the wind tunnel is indicated in figures 1 and 2.

Test Cylinder

In addition to the test cylinder, figure 1 also shows some of the auxiliary apparatus necessary to precool the cylinder. The principal part of the cooling apparatus was a sleeve which is illustrated in the retracted position and which is also shown by phantom lines in the forward cooling position. When retracted, the sleeve exposed over a 4-foot length of the 4-inch-diameter cylinder on which heat-transfer measurements could be made. The sleeve was actuated by a pneumatic cylinder and piston connected to the sleeve with a push-rod linkage.

When the cooling sleeve was in the forward position, a liquid-nitrogen inlet supply pipe on the tunnel side wall (shown in view A-A, fig. 1) engaged the supply pipe on the cooling sleeve. Liquid nitrogen at a pressure of about 100 pounds per square inch gage was introduced into the sleeve, filling the annulus between the test cylinder and the inner sleeve wall. Approximately 70 pounds of liquid nitrogen was required to cool the test cylinder to a temperature of about -350° F. The time required for this cooling operation was about 2 minutes. Thereupon the cooling sleeve was retracted, leaving the cooled cylinder exposed to the tunnel airstream. Sleeve retraction time was about 2 seconds.

The test cylinder was double-wall construction to minimize heat transfer from the internal flow through the cylinder (as were also the coolant supply lines and cooling sleeve just mentioned). The outer test surface was spun of Inconel and was finished to 0.038-inch thickness

±0.0005 inch, with about an 8-microinch surface irregularity. The inner support cylinder, which can be seen in view A-A of figure 1, was turned of machine steel and extended back to the support strut. The forward section of this inner support cylinder was of about 1/16-inch wall thickness; downstream of the test area its thickness was increased by increasing the outside diameter to that of the test cylinder. Together, both cylinders formed a long continuous tube on which the cooling sleeve could slide. Close-fitting Teflon seals were used as bearings at the ends of the sleeve. Figure 1 also shows the leading-edge rings that formed the various bluntness sizes and shapes. The rings were made of heat-treated tool steel and matched the test cylinder surface with a maximum irregularity of about 0.0005 inch.

The test cylinder was instrumented with 48 calibrated copper-constantan thermocouples soft-soldered into small holes drilled in the surface. The thermocouple wires were led out of the model through the annular space between the inner and outer cylinders. Small-gage wire (no. 30) was used to minimize any heat capacity or conduction effects, and the wire was routed through the annular opening in such a way as not to fall in line with the thermocouples. Static-pressure orifices were placed along a bottom generator of the test surface and consisted of 0.060-inch-outside-diameter, 0.010-inch-wall-thickness stainless steel tubing soft-soldered into the test surface. The tubes were bent at right angles to the surface and finished off flush. These tubes also were routed out through the annular space between the test and support cylinders.

Cone Model

Figure 2 shows the cone model in position in the 1- by 1-foot variable Reynolds number tunnel and also shows pertinent details of the cone tips used in the tests. The cone was spun of type-347 stainless steel with a wall thickness of 0.030 inch. The removable sharp-tip section (11.4 in. long) was hollow to facilitate instrumentation in the same manner as the aftersection of the cone. The shorter tips, however, were solid and were not instrumented.

Instrumentation for the cone model consisted of 42 calibrated constantan thermocouples at the spacings indicated in figure 2 (and fig. 8). No pressure instrumentation was provided; and, since no practical scheme for precooling the cone could be imagined in the present installation, it was used only for obtaining equilibrium temperature data.

Test Instrumentation and Procedure

The instrumentation used to obtain the equilibrium temperature distribution on the cone and cylinder models was a 2-millivolt-range self-balancing potentiometer recording on a punch tape through a digitizer. The individual thermocouples were cycled through automatically at a rate of about 1 or 2 per second. The final temperatures computed from this instrumentation were accurate to $\pm\frac{1}{2}^{\circ}$ F.

To obtain transient temperature records for computing heat-transfer rates, a 30-channel oscillograph recorder was used. Records of galvanometer deflection were run off at a paper speed of 1/2 inch per second. Temperature changes were sufficiently gradual so there was no question of adequate response time. Final temperatures computed from galvanometer traces were accurate to $\pm 2^{\circ}$ F, and transient temperature data were obtained on the cylinder model only.

Pressure distributions were measured on butylphthalate manometers. Only the results obtained at the high Reynolds numbers are presented, since it is only for these that response times were short enough to insure accurate pressure indications. For these conditions static-pressure errors were less than ±0.004 pound per square inch. Stagnation pressures were measured with precision pressure gages to an accuracy of ±0.1 pound per square inch.

Schlieren photographs were taken for both the equilibrium tests and the heat-transfer tests to obtain additional visual information. During the heat-up phase of the heat-transfer tests, similar photographs were taken at 6-second intervals. The schlieren exposures were of the order of 1 microsecond. In addition, some high-speed motion pictures were taken of the boundary layer for the equilibrium cylinder tests with the one-dimensional magnifying schlieren setup used in reference 5.

RESULTS

Pressure Distribution on Cylinder

Static-pressure distributions on the 4-inch cylinder are plotted in figure 3 in terms of pressure coefficient for the various bluntnesses. (Pressure coefficient accuracies, based on instrumentation errors, are about ±1 percent.) Near the leading edge, only the 0.060- and 0.151-inch bluntnesses are seen to depart from the essentially flat pressure distributions that were characteristic of the sharper leading-edge configurations. This leading-edge pressure rise for the larger bluntnesses was also observed in the Mach 3.1 tests reported in reference 3 and appears to be the recompression that normally follows the expansion

around a blunt leading edge. Evidence of this recompression is observed in schlieren photographs where a second compression shock originating 1 or 2 leading-edge bluntnesses downstream of the leading edge is formed. This second shock is most pronounced on the flat-blunted leading edge, as indicated in figure 4, where leading-edge shock configurations for sharp, 0.151-inch-round, and 0.151-inch-flat bluntnesses are shown.

Downstream of $x \approx 28$ inches, a rise in pressure is observed for the 0.060- and 0.151-inch bluntnesses which is caused by a reflection of the relatively strong leading-edge shock. (All symbols are defined in appendix A.) No data points for the sharper leading edges are shown in this region because a steadying support strut was attached to the cylinder at the time of these pressure measurements. This strut was used temporarily to determine whether model vibrations had a perceptible effect on the observed temperatures and transition positions. None could be found. Because the shock impingement for the sharper leading edges occurred at $x \approx 38$ inches and because no pressure fluctuations are visible far downstream, it is quite unlikely that the pressure distribution was anything but flat all along the cylinder for leading-edge thicknesses less than 0.010 inch.

Equilibrium Temperature Distribution on Cylinder

Equilibrium temperatures were measured on the cylinder model at a tunnel stagnation temperature of 250° F and at stagnation pressures of from 40 to 135 pounds per square inch absolute. At a Mach number of 4.95 these conditions gave a free-stream Reynolds number of from 1.3×10^5 to about 4.5×10^5 per inch. Each of the eight bluntnesses made for the cylinder model was tested under these flow conditions to determine the resulting temperature distribution on the cylinder surface.

In view of the large amount of experimental data, only those obtained at a unit Reynolds number of 4.5×10^5 per inch are presented to show the effect of bluntness on the equilibrium temperature distribution. Figure 5 shows these temperature distributions expressed in terms of the recovery factor η, which is defined

$$\eta = \frac{T_w - T_\infty}{T_0 - T_\infty}$$

Accuracy of the recovery factor results is considered in appendix B, where it is stated that the error in the recovery factors shown in figure 5 is ±3 percent in the laminar region and ±0.6 percent in the turbulent. No estimate of the error in the transitional (peak temperature) region has been made. Temperature distributions obtained at lower unit

Reynolds numbers followed trends similar to those in figure 5, except that the temperature peak at the transition point was displaced downstream.

Sharp-leading-edge case. - The theoretical laminar recovery factor, which for a flat plate is approximated by

$$\eta = \sqrt{Pr}$$

where $Pr = 0.693$ (based on a wall temperature of 640° R) is found to be 0.833 and is indicated in figure 5 by a dark horizontal line. This value of η defines a lower limit that the experimental data never reached, presumably because of heat conduction in the solid leading edge from the internal flow through the cylinder. In fact, if the temperature of the leading edge is taken as the average of the theoretical recovery temperatures inside and outside of the leading-edge wedge and an average recovery factor is computed, it is found to be 0.844 - which is the experimental value found for the sharp leading edge at $x = 2$ inches.

A comparison of the turbulent recovery factors obtained with leading edges ≤0.010 inch in figure 5 shows that the commonly used empirical approximation

$$\eta = \sqrt[3]{Pr} = \sqrt[3]{0.693} = 0.885$$

does not agree well with the experimental results, which average out at about 0.875. Hence, a tentative value of 0.875 will be used as a reference value of the recovery factor for the sharp-leading-edge cylinder in the subsequent discussions. This value is also indicated in figure 5 by a dark horizontal line.

Effect of leading-edge bluntness. - Two of the most conspicuous effects of blunting the leading edge are the general rise in recovery factor level and the downstream displacement of the transition point (indicated by the temperature peak). Both of these effects can be seen in figure 5 and are consequences of the formation of a shock layer (also termed an inviscid shear layer), which is due to a detached shock at the blunted leading edge (ref. 2). The shock layer is a region of reduced velocity and density adjacent to the body surface, the thickness of this layer being proportional to the leading-edge bluntness.

The shape and size of the shock-layer profiles for the 0.020- and 0.151-inch round bluntnesses are shown in figure 6, together with the accompanying boundary-layer developments. The shock-layer profiles were obtained from reference 2, and the adjusted boundary-layer thickness $\delta - \delta^*$ is based on the low velocity-density conditions that prevail at the wall in the presence of the shock layer. Reference 6 was used to compute the laminar-boundary-layer thickness at edge conditions

corresponding to the highest and lowest unit Reynolds numbers of the test; that is, $u_\infty/\nu_\infty = 1.5$ and 4.5×10^5 per inch. Use of an adjusted boundary-layer thickness $\delta - \delta^*$ takes into account the outward displacement of the shock layer by the boundary layer, and makes a direct comparison between the outer edge of the boundary layer and the shock layer possible without correcting the computed shock-layer thicknesses of reference 2.

Figure 6 shows that the laminar-boundary-layer development for both the high and low unit Reynolds numbers is well within the low-velocity part of the shock layer for the 0.151-inch bluntness over the entire model. Similarly, the boundary-layer development is confined to the lower Mach number parts of the shock layer even for the 0.020-inch bluntness under some conditions. This is shown to be the case at the highest unit Reynolds number, where the peak temperature occurs at 13 inches from the leading edge (fig. 5) and the laminar boundary layer has an edge Mach number of 3.35 (fig. 6). The surface temperature downstream of the temperature peak drops considerably faster for the 0.020-inch leading edge than for the 0.151 because of the much thinner shock layer in the first instance (fig. 5).

The increase in the recovery factor level with increasing bluntness for either the laminar or the turbulent boundary layer is a result of the decrease in Mach number at the outer edge of the boundary layer, which in turn depends on the shock-layer thickness. The maximum recovery factor for the laminar, turbulent, or transitional boundary layer will be reached when the outer edge of the boundary layer sees the minimum value of the Mach number, which happens to be 2.92 for the present tests. For these conditions the adiabatic wall temperature may be given by

$$\frac{T_{aw}}{T_0} = \frac{1 + \eta'\left(\frac{\gamma - 1}{2}\right)M_e^2}{1 + \left(\frac{\gamma - 1}{2}\right)M_e^2}$$

where $\eta' = 0.833$ for laminar flow and 0.875 for turbulent and where $M_e = 2.92$. The preceding value for T_{aw}/T_0 may be incorporated into the definition of recovery factor based on free-stream conditions, which is plotted in figure 5:

$$\eta = \frac{T_{aw}/T_0 - T_\infty/T_0}{1 - T_\infty/T_0} \qquad (1)$$

Substituting $T_\infty/T_0 = 0.1667$, which corresponds to $M_\infty = 5$, yields $\eta = 0.874$ for laminar flow and 0.908 for turbulent. These two values are indicated in figure 5 by dark horizontal lines.

It should be noted that these values of η are the highest values that can be obtained from the shock-layer assumptions, excluding the transition region, and that they presume the shock layer to be much thicker than the boundary layer at the point in question. Actually, all the values between η' and η are possible, depending on the relative thicknesses of the shock layer and the boundary layer.

Experimental recovery factors in figure 5 are seen to increase with increasing bluntness, the increases being most prominent with small bluntnesses in the laminar region and extending into the turbulent when the bluntness is sufficiently large. In the laminar region, however, these increases exceed the theoretical value of 0.874. These large recovery factors no doubt have their origin in the conduction and convection of heat from the blunted leading-edge ring, which is near to the stagnation temperature. In the turbulent region the recovery factor measured for the blunt condition has an average value of 0.912, which is slightly above the predicted value of 0.908 for the blunt case. Reduction in the measured value by the estimated experimental error (appendix B) yields a corrected measured value of 0.907, which compares favorably with the predicted value, 0.908.

Peak temperature and transition. - Earlier equilibrium temperature measurements at Mach 3.12 (ref. 3) and experiments by other workers on zero pressure gradient bodies (e.g., ref. 7) have indicated that the location of the peak temperature correlates closely with the point of transition observed in schlieren photographs. Results of the present experiment also indicate this to be true for leading edges of <0.001- and 0.005-inch (see fig. 5). However, the temperature peak for the 0.010-inch leading edge appeared 2 inches upstream of the schlieren location, and that for the 0.020-inch leading edge was 4 inches upstream and decreased somewhat for larger bluntnesses. An explanation for this discrepancy may be apparent if the radial heat conduction is taken into account as discussed in appendix B. Thus, the equilibrium temperature distribution of the inner cylinder is transmitted in part to the outer test surface by conduction through the insulating layer. If the transition point on the inner cylinder is slightly upstream or downstream of that on the outer cylinder, or if some other temperature disturbance is present on the inner cylinder, then the effect will be to shift the outer temperature peak somewhat. If the two temperature peaks are widely separated, as with the larger bluntnesses, the peaks will tend to remain more distinct. The jog in the distributions at $x \approx 38$ inches, however, is the result of the leading-edge shock that reflects off the tunnel wall. In view of the ease with which a transition temperature peak may be followed from the temperature distributions, and the general agreement with available schlieren photographs, the peak has been chosen to be indicative of the transition point.

Accordingly, in figure 7 are plotted the locations of the peak temperature given in terms of the dimensionless Reynolds number $(u_\infty x_p)/\nu_\infty$. These are given as a function of u_∞/ν_∞ with the leading-edge bluntness as parameter. Figure 7 indicates very large delays in transition location, particularly for slight increases in bluntness over the sharp condition. In the larger bluntnesses beneficial effects of rounded bluntness over the flat are also apparent. Both of these trends were observed in the Mach 3.1 bluntness results reported in reference 3.

The ratio of transition location with large bluntness to that in the sharp condition is about 3.0 over the entire unit Reynolds number range, according to figure 7. This ratio is to be compared with a theoretical ratio suggested in reference 2, namely, the inverse of the ratio of unit Reynolds number in the blunted condition to the sharp. For a free-stream Mach number of 5 this inverse ratio is about 4.4, according to reference 2. The calculated value of 4.4, however, disregards any effect that the unit Reynolds number has on the transition Reynolds number when the leading edge is sharp, as well as any effect of the decreased outer-edge Mach number which the boundary layer has on the transition Reynolds number. If the effect of unit Reynolds number on the value 4.4 is computed by using the sharp-leading-edge results of figure 7, a 50-percent reduction is easily possible, bringing the inverse ratio down to about 2.2, compared with an experimental value of 3.0. A further correction for the effect of reduced Mach number can be estimated from the Mach 3.12 experimental results of reference 3. Reference 3 gives a transition Reynolds number for a sharp cylinder at high values of u_∞/ν_∞ of $Re_{x,t} = 2\times10^6$ compared with 2.4×10^6 for the present results. Thus, the inverse ratio of 2.2 is further reduced to about 1.8.

The preceding calculations are really only conjectures as to the effect of changes in gross flow characteristics. It is entirely possible that larger transition Reynolds numbers may have been obtainable had it been possible to test larger leading-edge bluntnesses. Such tests were not possible, since a further increase in leading-edge bluntness caused spillage of flow around the leading edge which tended to destabilize the boundary layer.

A comparison of the present transition delays with those obtained at Mach 3.1 in reference 3 is of interest. At Mach 3.1 transition was moved downstream by a factor of about 2.4 for a cylinder having 0.096-inch bluntness, whereas a comparable bluntness in the present tests would give about 3.0. The inverse of the unit Reynolds number ratio at Mach 3.1 is about 2.2, which is to be compared with 4.4 at Mach 5.0.

Equilibrium Temperature Distribution on Cone

Sharp-tip results. - The recovery distributions obtained on the conical model with a sharp tip and with 0.5- and 1.0-inch bluntnesses are shown in figure 8 at a unit Reynolds number of 4.5×10^5 per inch. The recovery factor distributions follow the same general trends noted on the cylinder model, except that the distributions are smoother and the temperature peaks are sharp. Also, there is a close correspondence between schlieren observations (indicated by a short vertical line through a data symbol) and temperature peaks. A comparison of the theoretical recovery factors in the laminar region shows a value of 0.833 for theory (based on properties at the wall) and about 0.835 for the measured value when a sharp tip is used. Turbulent recovery factors vary from about 0.878 just downstream of the temperature peak to 0.867 near the base of the model. There does appear a plateau in the distribution at about $\eta = 0.875$, which is the turbulent value found on the cylinder. The gradual drop as the base of the model is approached may be related to low temperatures on the base flange, these low temperatures making themselves felt through eddy currents inside the model and conduction in the skin. Because of the small cone angle, there was no conical shock visible in any schlieren photographs and apparently no problem with a shock reflected from the tunnel walls, which would thereby affect the temperature distribution on the cone.

Effect of tip bluntness. - Laminar recovery factors obtained with the 1-inch tip bluntness measured 0.870, which compares favorably with a theoretically maximum possible value of 0.874, based on Mach 2.92 in the shock layer and equation (1). The maximum turbulent recovery factor for the same bluntness measured about 0.900 compared with a theoretical maximum value of 0.908. The measured value 0.900 was observed only immediately after the transition peak; thereafter, a rather rapid drop in the turbulent recovery temperature followed. An almost parallel but earlier drop can be seen for the 0.5-inch-bluntness cone. These drops in recovery temperature and their relation to each other may be explainable in terms of the relative thicknesses of the boundary layer and shock layer in the turbulent region.

Peak temperature and transition on the cone. - Figure 9 presents the locations of the peak temperatures on the cone in terms of the Reynolds number, similar to the plot for the cylinder in figure 7. In addition, some data which show an effect of cone longitudinal location in the wind tunnel test section are presented.

Figure 9 shows increasing transition delays with increasing bluntness, but of a smaller magnitude than found for the cylinder. A comparison of the largest bluntness transition location with that observed for the sharp cone reveals a blunted-to-sharp transition ratio of 2.1 at the largest unit Reynolds number and 1.6 at the lowest. These values

are to be compared with the experimental value of 3.0 found for the cylinder and to the theoretical value of 4.4 suggested in reference 2. Similarly, reduced effectiveness of bluntness on a cone compared with a cylinder was found at Mach 3.1 in reference 3.

A reason that suggests itself for the reduced effectiveness of the bluntness on the cone is the thinning of the shock layer with increasing distance from the tip. Figure 10 shows the shock-layer thickness distribution at the Mach 3.35 streamline (which is about the boundary of the lower quarter of the shock layer) for the 0.5- and 1.0-inch bluntnesses. Also shown is the adjusted boundary-layer thickness $\delta - \delta^*$ based on conditions at the wall in the shock layer, assuming the body to be a (sharp) cone. It is apparent that for the 1.0-inch bluntness the boundary layer does not penetrate the lower shock layer until $x = 31$ inches at $u_\infty/\nu_\infty = 4.5\times10^5$ per inch. The transition location for these conditions is, according to figure 8, 15 inches. In other words, the transition delay should be a maximum, and no further benefits are to be expected by increasing the bluntness in this instance. For the lowest unit Reynolds number, where the distance to transition is about 25 inches, the point of intersection of the boundary layer with the shock layer is found to be 25 inches also, as may be verified in figure 10. In making these comparisons, it should be borne in mind that the boundary-layer calculations for figure 10 were made with the assumption of conical flow beginning at the tip. In all likelihood the boundary-layer thickness should be larger than shown and should approach the flat-plate boundary layer of figure 6 as the bluntness is increased. In this case the boundary layer would emerge from the shock layer shown upstream of the transition point (for $u_\infty/\nu_\infty = 1.5\times10^5$/in.), and some additional transition delay may be possible with increasing bluntness at the lower unit Reynolds numbers.

An additional result to be noted in figure 9 is the increase in peak Reynolds number (13 percent) as the model was translated to a new position $6\frac{1}{4}$ inches upstream in the tunnel. A similar displacement of the transition point had been observed on numerous occasions at Mach 3.1 for various body shapes. Such a behavior of the transition point is indicative of a decreasing turbulence level farther upstream, perhaps due to the decreased tunnel wall boundary-layer thickness. It also suggests that, had the blunted cone been translated forward so that its tip always occupied the same position as that for the sharp tip, then larger transition delays with bluntness would have resulted.

Cylinder Heat Transfer

Calculation procedure. - Heat transfer to the test surface of the cylinder was computed from the transient-heat-capacity equation

$$q = (c\rho\tau)_w \frac{dT_w}{dt}$$

where q is the total (convected, conducted, radiated, etc.) heat transfer per unit area of test surface, $c = c(T_w)$ is the specific heat of the wall material, ρ is the wall density, τ the wall thickness, and dT_w/dt the derivative of the wall temperature with time. If q may be considered to be only convected heat, then the dimensionless heat-transfer coefficient, Stanton number, may be written as

$$St = \frac{(c\rho\tau)_w}{(c_p\rho u)_\infty} \frac{dT_w/dt}{T_{aw} - T_w} \tag{2}$$

where $(c_p\rho u)_\infty$ represents the constant pressure specific heat, the density, and the velocity of the free stream. The quantity T_{aw} is the adiabatic wall temperature, which, to simplify calculations, was assumed to be equal to 0.9 of the total temperature for the laminar, transitional, and turbulent flow regions.

Wall temperatures T_w and time derivatives dT_w/dt were determined from oscillograph records of galvanometer deflections as a function of time. Derivatives were obtained from the best fit of five points to a parabola. These points were spaced at 2-, 5-, or 10-second intervals, the smaller intervals being used for the larger derivatives in order to maintain uniform accuracy.

Errors and corrections. - Appendix B contains an analysis of errors resulting either from instrumentation and calculational procedure or from assumptions regarding the physical phenomena. Included in the former group are potentiometer and galvanometer errors, calibration errors, and oscillograph trace measurement errors. In the latter group are adiabatic wall temperature assumptions, axial and radial heat conduction, nonconductive effects of wall temperature variation, and unaccounted-for variations in test wall thickness. Errors arising from the latter group in general are quite difficult to assess and often involve prohibitive time to evaluate at each test point, or in some instances are impossible to evaluate. In addition, many of the effects listed may be concurrent and mutually interacting, and some are impossible to estimate except for idealized situations - for example, phenomena in the transition region. For this reason the heat-transfer results (Stanton number) are given in their uncorrected form with the intention that a rough error estimate be mentally applied - one for the predominantly laminar boundary layer, and another for the predominantly turbulent. These rough estimates are:

In the laminar region, the error in the experimental points is
+20 ±6 percent at $u_\infty/\nu_\infty = 4.5\times10^5$/in.
+32 ±6 percent at $u_\infty/\nu_\infty = 1.5\times10^5$/in.

In the turbulent region,
+9 ±6 percent at $u_\infty/\nu_\infty = 4.5\times10^5$/in.
+21 ±6 percent at $u_\infty/\nu_\infty = 1.5\times10^5$/in.

Based on the large magnitude of some of these errors, it was decided to withhold all heat-transfer results except those for the highest unit Reynolds number (4.5×10^5/in.). Another deletion was made in discarding all results that contained an error greater than ±5 percent due to the approximation of adiabatic wall temperature, $T_{aw} = 0.9\ T_0$.

Heat-transfer results. - Plots of the Stanton number as a function of the Reynolds number $(u_\infty x)/\nu_\infty$, with time as a parameter, are presented in figures 11 to 13 for the sharp, 0.020-inch-, and 0.151-inch-blunt leading edges at $u_\infty/\nu_\infty = 4.5\times10^5$ per inch. In addition, theoretical flat-plate laminar (ref. 6) and turbulent (ref. 8) heat-transfer coefficients at $M_\infty = 4.95$ are shown for comparison. The laminar coefficients shown are for temperature ratios $T_w/T_\infty = 1.0$ and 5.2, which were the extreme conditions possible using liquid nitrogen as a coolant as one extreme and the adiabatic wall temperature as the other. The turbulent Stanton numbers have a wider spread with wall temperature ratio, and have therefore been given at temperature ratios 1, 2, 3, 4, 5, and 5.2. Ratios of wall to stream temperature T_w/T_∞ are listed for the various times so that a comparison with the theoretical values can be made. These values of T_w/T_∞ are calculated at the start of the turbulent run.

Heat transfer when the leading edge is sharp. - The sharp-leading-edge results presented in figure 11 indicate experimental heat-transfer coefficients appreciably larger then theoretical, particularly in the laminar region. The variation of Stanton number with wall temperature ratio T_w/T_∞ in the turbulent case, however, is approximately the range given by theory. If it is assumed that the experimental errors calculated in appendix B, +20 percent in the laminar and +9 percent in the turbulent region, are applicable, the measured heat-transfer rates still exceed the theoretical by some 200 percent in the laminar region and 10 to 15 percent in the turbulent.

The reason for the large discrepancies between experiment and theory in the laminar region, even after the errors have been deducted from the experimental results, follows from use of the wrong corrections. In appendix B, a +10-percent error is assigned to the experimental laminar points to account for the effect of a nonuniform surface temperature on

the convective heat-transfer coefficient. This error, as pointed out, applies only at $x \geq 6$ inches; at x values near to the leading edge it becomes quite large, and at $x = 3$ inches, which corresponds to a Reynolds number of 1.33×10^6 in figure 11, it reaches 186 percent. Such a reduction in Stanton number for the first three points results in acceptable agreement with theory, although it should be remembered that it is not certain that the first group of points is wholly laminar. Very likely, the second group of points at a Reynolds number of 2.23×10^6 is transitional and may not have a large error associated with it.

The 10- to 15-percent discrepancy between experiment and theory which remains in the turbulent case, even after the 9-percent experimental correction has been allowed, can be readily accounted for if the Reynolds number in the abscissa is based on a length reckoned from the start of the turbulent boundary layer rather than from the leading edge of the cylinder. A good approximation for the start of the turbulent layer appears to be a Reynolds number of 3.2×10^6, according to figure 11. Subtraction of 3.2×10^6 from the abscissa of the experimental points results in the plot shown in figure 14. Subtraction of the 9-percent average correction computed for the turbulent case from the ordinate results in acceptable agreement between experiment and theory.

Heat-transfer measurements were also made at unit Reynolds numbers of 3.2, 2.2, and 1.5×10^5 per inch by reducing the tunnel pressure level. These results have not been included, as is stated elsewhere, because the corrections necessary became prohibitively large at the lower unit Reynolds numbers. It should be added, however, that in all cases the application of the estimated correction factor brought the experimental results into good agreement with both the laminar theory of reference 6 and the turbulent theory of reference 8. In one sense, however, the lower unit Reynolds numbers permitted a more extensive laminar run and a somewhat better check on laminar theory.

Heat transfer with bluntness. - Heat-transfer measurements similar to those described for the sharp-edged cylinder were also made for two values of the bluntness, 0.020-inch flat and 0.151-inch round. The results obtained at unit Reynolds numbers of about 4.5×10^5 per inch are shown in figures 12 and 13. The trends of the experimental points in these figures exhibit the characteristic laminar-transitional-turbulent shape also found in figure 11. It is apparent, however, that the laminar region becomes longer and the transitional region is displaced downstream as the bluntness is increased. Thus, the present heat-transfer results corroborate the trends of earlier tests (refs. 1 and 3), which used only schlieren and equilibrium surface temperatures as a means of detecting transition when the leading edge was blunted.

In addition, the results of figures 12 and 13 show substantial departures from the theoretical curves in both the laminar and the

turbulent regions. The Stanton numbers in figures 12 and 13, however, are based on an outer-edge Mach number of 5 and do not take into account reductions in the unit Reynolds number that take place in the shock layer. In this sense, experiment and theory are not strictly comparable in figures 12 and 13.

In order to have a more meaningful comparison between experiment and theory, it is expedient to consider only the results for the 0.151-inch bluntness. For this case the boundary layer may be considered to be within the low-speed part of the shock layer throughout its entire development (according to fig. 6). The Stanton number will then be given by

$$St = \frac{q}{T_{aw} - T_w} \frac{1}{(\rho u c_p)_e}$$

where, for conditions at the wall in the shock layer,

$$\frac{(\rho u c_p)_e}{(\rho u c_p)_\infty} = \frac{M_e}{M_\infty} \sqrt{\frac{1 + \frac{\gamma - 1}{2} M_e^2}{1 + \frac{\gamma - 1}{2} M_\infty^2}} = 0.392.$$

Likewise, there will be a reduction in the unit Reynolds number, which according to reference 2 will be

$$\frac{(u/\nu)_e}{(u/\nu)_\infty} = 0.228$$

Figure 15 presents the experimental results for the 0.151-inch bluntness of figure 13 with the Stanton number and Reynolds number corrected according to the foregoing scheme. It also presents the theoretical laminar and turbulent Stanton numbers for Mach 2.92 instead of 5.0. Figure 15 shows discrepancies considerably greater in both the laminar and turbulent regions than those occurring in figure 13. None of the estimated corrections of appendix B is large enough to bring the experimental results into approximate agreement with the theory. It is probable that at least one of two conclusions must follow: (1) that the boundary layer in the blunt case does not follow the simple picture of a boundary layer developing in a uniform, well-behaved shear layer with a Mach number and Reynolds number appropriate to the shear layer, or (2) that extraneous heat-transfer effects not taken into account in appendix B exist. These conclusions apply to figure 15 and probably in large part would also apply to the heat-transfer results obtained for the 0.020-inch bluntness.

In summary, it may be stated that the measured heat transfer for the sharp-leading-edge model is in agreement with theory when suitable corrections for extraneous effects are made. The addition of leading-edge bluntness makes possible reductions in heat transfer, apparently by increasing the transition Reynolds number; however, an understanding of the exact heat-transfer mechanism in this case is lacking.

Transition on the Cylinder With and Without Bluntness

It has been shown that the schlieren, equilibrium surface temperature, and heat-transfer methods all indicate increasing transition Reynolds numbers with increasing leading-edge bluntness. It is of interest to determine how closely the three methods agree with one another. Included in figures 11 to 13 are symbols that indicate transition locations as determined from schlieren and peak temperature locations. Both the schlieren and the peak temperature methods show transition occurring prior to, or in the region of, rising heat transfer. Implicit in this comparison is that the transition locations found from the heat-transfer results do not depend strongly on wall temperature levels, since the schlieren and equilibrium surface temperature methods give transition locations for the adiabatic wall condition only.

Ordinarily it should be possible to examine figures 11 to 13 (or, better yet, the original oscillograph traces) and determine the effect of temperature level on the transition location (cf., ref. 9). Both of these methods were used in the present instance; but neither revealed a definite, systematic variation in transition location with wall temperature, which is plotted in figure 16. Transition was chosen for figure 16 as the position of the first data point in the transition region of the heat-transfer plots, that is, the first point that reverses the downward trend of the laminar data. In addition to the results shown in figures 11 to 13, nine other sets of heat-transfer data not included in this report were used. These other heat-transfer data were obtained at three lower unit Reynolds numbers, and all are identified in figure 16.

Figure 16 shows the transition location in terms of the ratio x_t/x_{t_0}, where x_t is the distance to the transition point at a given wall temperature and x_{t_0} is the distance at a temperature near to equilibrium. For temperature ratios greater than 2.5 there is no effect of temperature level on transition locations, regardless of unit Reynolds number or bluntness. At temperature ratios less than 2.5 the length of laminar run for the sharp leading edge either remains a constant or increases slightly as the temperature is lowered. This behavior is to be contrasted to the large transition delays observed at low surface temperatures on conical-type bodies at Mach 3.1 reported in reference 9.

The 0.020- and 0.151-inch leading-edge models, however, show a somewhat different behavior. With decreases in temperature ratio below 2.5, the laminar run may first increase and then diminish, or it may simply decrease when the temperature ratio becomes low enough. This reduction resembles the phenomenon known as "transition reversal," described in reference 9. Like the transition reversal of reference 9, which is well documented, the present behavior is most characteristic of the larger bluntnesses and is difficult, if not impossible, to detect when the leading edge is sharp. A study of schlieren photographs taken during the heat-transfer process reveals certain characteristics of the flow that may explain the apparent transition reversal in the present case. During the initial period of the heat transfer, that is, until the cooling cylinder reached its final rest position $4\frac{1}{2}$ feet downstream, spillage of some of the internal flow around the leading edge occurred. The spillage was caused by the cooling cylinder covering up certain internal-flow relief vents until the outer cylinder reached its final rest position.

The initial spillage at the leading edge is indicated in the schlieren photographs shown in figure 17. Shown is the cylinder with the sharp leading edge, the leading-edge shock being initially detached due to spillage (fig. 17(a)) and $1\frac{1}{2}$ seconds later reaching its final steady-state attached condition (fig. 17(b)). The sharp-leading-edge cylinder was chosen for illustration because these two conditions of the flow are outstanding in this instance. In the blunt condition the leading-edge shock was detached in both the initial and the final configurations, the detachment in the initial condition being significantly larger than in the final. The increase in the heat transfer in the detached condition when the leading edge was blunted was never great, indicating primarily a slight change in the heat-transfer mechanism rather than the difference between laminar and turbulent flow. For the sharp leading edge, the spillage had no detectable effect on the heat-transfer or transition location. From these observations it may be inferred that transition reversal, as found in reference 9, did not occur in the present tests.

SCHLIEREN RESULTS

Transition locations found from short-exposure schlieren photographs have already been indicated (see figs. 5, 8, 11 to 13). Evidence of flow spillage at the leading edge during the first 1 or 2 seconds of exposure of the cooled cylinder to the hot airstream also has been presented. In addition to these observations, high-speed motion pictures (4000 frames/sec) were taken to investigate the possibility of unsteadiness associated with the transition region for the case of zero heat transfer. In comparing the present high-speed motion pictures with those taken in earlier tests at Mach 3.1 (ref. 5), the outstanding differences appeared

to be in a decreased fluctuation of the flow in the transition region. At Mach 3.1 an unsteadiness of the boundary layer in the transition region (which resembled intermittent separation of the flow) was quite apparent. In the present tests this unsteadiness was almost nonexistent.

CONCLUSIONS

E-797

Schlieren, heat-transfer, and surface temperature measurements were made on a hollow cylinder and a cone at a Mach number of 4.95 in the Reynolds number range 1.5×10^5 to 4.5×10^5 per inch. These tests showed:

1. In the zero heat-transfer condition the surface recovery temperature on the sharp cylinder varied from a near-laminar initial value to a peak value in the transition region, and finally to a turbulent recovery value. Recovery temperatures in the blunted condition were generally higher, and the peak, or transition, region was displaced downstream. The length of the laminar run was tripled on the cylinder by the use of a 0.151-inch blunt leading edge, compared with the sharp. Using a 1-inch bluntness on the cone resulted in transition delays of 1.6 to 2.1 times the sharp cone value. The present transition delays are larger than those found in earlier tests at Mach 3.1, these trends being in harmony with Moeckel's shock-layer analysis.

2. The sharp-leading-edge heat-transfer measurements, when suitably corrected, were found to agree well with Van Driest's theory in the turbulent region. Because of the largeness of the corrections in the laminar region, a more qualified agreement with theory must be given. The heat-transfer measurements, like the recovery temperature measurements, indicated large downstream movements of the transition region and sizeable reductions in heat transfer due to bluntness. These transition movements indicated no dependence on the surface temperatures at temperature levels above wall to free-stream temperature ratios greater than 2.5. Below this temperature level the sharp-leading-edge configuration showed a slight increase in distance to transition; the blunt-leading-edge configuration usually indicated a decrease (although this behavior was somewhat erratic).

3. From a comparison of transition locations observed with schlieren photography, peak temperature locations, and a rise in heat transfer, it was concluded that all three methods were in substantial agreement. The commonly used schlieren and temperature peak methods indicated a point just downstream of the minimum laminar heat transfer and prior to the rapid rise preceding the turbulent flow region.

Lewis Research Center
National Aeronautics and Space Administration
Cleveland, Ohio, June 1, 1961

APPENDIX A

SYMBOLS

The following symbols were used in this report:

c	specific heat (of metal wall)
c_p	specific heat at constant pressure (air)
h	heat-transfer coefficient, $q/\Delta T$
k	thermal conductivity
M	Mach number
Pr	Prandtl number
p	static pressure
q	rate of heat flow
Re_x	Reynolds number based on length of run
St	Stanton number, $h/(\rho u c_p)$
T	temperature
t	time
u	x-component of velocity
x	distance from leading edge of cylinder or tip of cone, along generator
y	distance normal to cylinder or cone surface
γ	specific heat ratio, c_p/c_v
δ	boundary-layer thickness
δ^*	displacement thickness of boundary layer
$\delta - \delta^*$	adjusted boundary-layer thickness
η	temperature recovery factor

ν	kinetic viscosity
ρ	density
τ	thickness of test wall

Subscripts:

aw	adiabatic wall condition
e	condition at edge of boundary layer that is developing in a relatively thick shear layer
eq	equilibrium temperature condition
p	peak temperature condition
t	condition at transition point
w	wall condition
∞	free-stream condition
0	stagnation condition
1	outer cylinder shell
2	inner cylinder shell

APPENDIX B

ANALYSIS OF HEAT-TRANSFER ERRORS

The results presented in this report are subject to two basic types of error: (1) error due to instrumentation and calculation procedure, and (2) error due to assumptions regarding the measured phenomena. The first type of error already has been considered in the section describing the experimental setup and techniques, where errors of $\pm 1/2^{\circ}$ F were reported for the equilibrium temperature measurements and $\pm 2^{\circ}$ F for the transient temperature. In addition, there are computational errors that may reach ±3 percent in the determination of the temperature-time slope. This latter error affects only the heat-transfer results. The second basic type of error, which results from assumptions regarding the nature of the experiment, is discussed next. These are errors in temperature potential, variations in test-surface thickness, amount of longitudinal heat conduction, radial heat leakage through test surface, assumption of constant wall temperature in computing the Stanton number, and heat loss by radiation.

Temperature Potential

To compute the heat-transfer coefficient from equation (2), page 13, the temperature potential $T_{aw} - T_w$ is required. The value of the adiabatic wall temperature T_{aw} was taken as 0.9 times the stream stagnation temperature T_0 in order to simplify the calculations. At the Mach number of the free stream, the true laminar value would be 0.8715 T_0 and the true turbulent value would be 0.9005 T_0. At the Mach number of the outer edge of the boundary layer (Mach 2.92) for the full-blunted condition, the value of T_{aw} would be 0.9026 T_0 and 0.9246 T_0 for laminar and turbulent flow, respectively. In addition, the adiabatic wall temperature has a smooth variation in the region between the laminar and turbulent flow with a peak value that is larger than even the turbulent value. Often this transition region is very extensive, making a unique value of T_{aw} necessary at every point. To make matters even more difficult, the transition region moves somewhat as the model becomes warmer, making it difficult to define an adiabatic wall temperature over a region of the test surface. In view of these difficulties, the adiabatic wall temperature was taken as 0.9 T_0. No heat-transfer calculations that had an error greater than 10 percent because of inaccuracy in T_{aw} were included in the report. In fact, the vast majority of the results had inaccuracies less than ±5 percent because of the approximation of the adiabatic wall temperature.

Test-Surface Thickness

A second assumption was made in using an average thickness for the test surface. The maximum variations in thickness above and below a mean value of 0.0385 inch were 0.001 inch, which means that the maximum possible error from this source is less than ±3 percent.

Heat Conduction in Test Surface

Another source of error stems from the assumption of zero heat conduction in the plate surface in an axial direction. This error is difficult to assess, particularly in the case of zero heat transfer (equilibrium results). Any attempt to compute the effect of conduction on the equilibrium test data is itself besought with assumptions, particularly in the transition region. Such a calculation was made in reference 5 at Mach 3.1. In the strictly laminar region, that is, halfway to the temperature peak, conduction effects were found to be small (<1 or 2 percent). Farther into the temperature peak region, the effect of conduction appeared to increase, but the magnitude of the effect was debatable.

An analysis of the axial heat-conduction effect in the transient heat-transfer tests was made for a number of longitudinal temperature distributions at a test time of $t = 14$ seconds. A section of the test surface showing the heat fluxes Q per unit width of surface is sketched as follows:

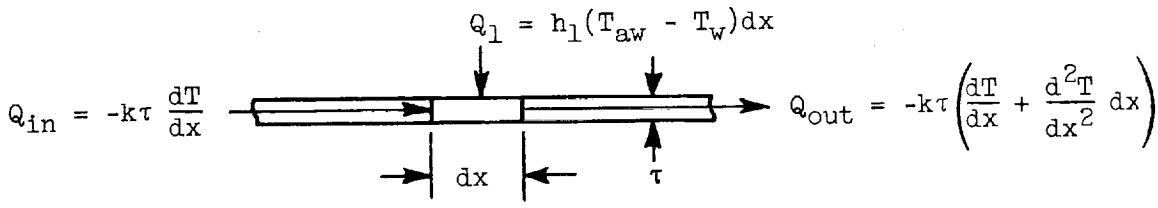

where h_l is the convective heat-transfer coefficient, k the surface material conductivity, and τ the surface thickness. If the plate is considered insulated on its lower surface, the true heat convection expressed in terms of the Stanton number may be written

$$St_{true} = St_{meas} - \frac{k_w \tau_w}{(c_p \rho u)_\infty} \frac{d^2T}{dx^2} \frac{1}{T_{aw} - T_w}$$

or, as the ratio of the true Stanton number to the measured,

$$\frac{St_{true}}{St_{meas}} = 1 - \left(\frac{k}{c_p\rho}\right)_w \frac{\frac{d^2T}{dx^2}}{\frac{dT}{dt}}$$

Calculations of St_{true}/St_{meas} were made along the test surface at $t = 14$ seconds for the temperature distributions shown in figure 18. These distributions embodied the most severe temperature changes observed in the tests and therefore represent the largest axial conduction error observed. This error had a maximum value of ± 1 percent at a distance of 1 to 2 inches from the leading edge.

Radial Heat Leakage

Another conduction correction that must be taken into account is the heat leakage from the inner to the outer cylinder across the insulating air gap. This heat leakage will result from the temperature difference between the inner and outer cylinders and is indicated by q_3 in the following sketch. For simplicity, the analysis of the radial heat leakage is assumed to be steady; and, as a consequence, q_3 is equal to q_2.

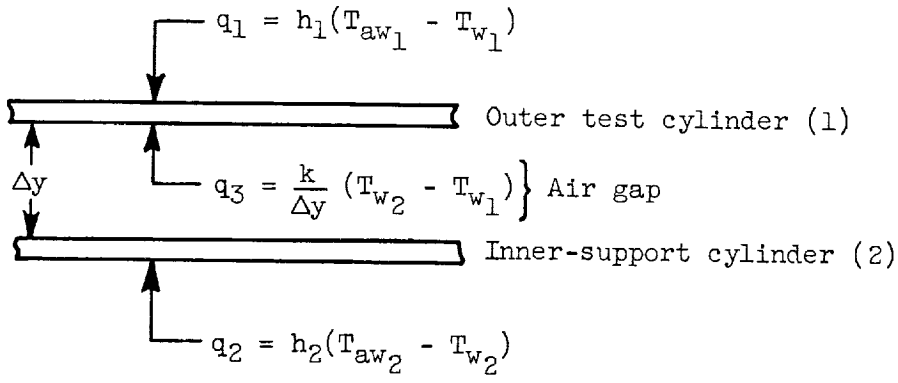

Assuming that the flow through the inner cylinder is governed by the isentropic area relations, it is found that the internal Mach number M_2 is 4.69 when the external Mach number M_1 is 4.95. For these conditions the internal and external cylinder recovery temperatures are practically equal, even though one may be laminar and the other turbulent. Thus,

$$T_{aw_1} = T_{aw_2} = T_{aw}$$

and the heat-transfer equations may be written:

$$q_1 = h_1(T_{aw} - T_{w_1})$$

$$q_2 = h_1\left(\frac{h_2}{h_1}\right)(T_{aw} - T_{w_2})$$

Subtracting these two equations and using the following relation for q_2,

$$q_2 = \frac{k}{\Delta y}(T_{w_2} - T_{w_1})$$

yields

$$\frac{q_1}{q_2} = \frac{h_1}{h_2} + \frac{h_1 \Delta y}{k}$$

The ratio $\frac{h_1}{h_2}$, based on flow conditions outside and inside the cylinders, is

$$\frac{h_1}{h_2} = 0.939 \text{ for laminar flow}$$

and

$$\frac{h_1}{h_2} = 1.124 \text{ for turbulent flow}$$

at a Reynolds number of 10^7. Actually, a value $h_1/h_2 = 1$ would be consistent with the accuracy of the assumptions made in the analysis. The ratio of the corrected to the measured heat transfer is given by

$$\frac{q_{corr}}{q_{meas}} = \frac{q_1}{q_1 + q_2} = \frac{\frac{q_1}{q_2}}{\frac{q_1}{q_2} + 1}$$

which is also a statement of the Stanton number ratio St_{corr}/St_{meas}. Using the theoretical Stanton numbers given in figures 11 to 13, it is

possible to determine h_1 for laminar and turbulent flows. Accordingly, the Stanton number ratio has been computed, and the results are plotted in figure 19 against the Reynolds number for laminar and turbulent flows.

The results shown in figure 19 indicate a larger effect of heat leakage for laminar than for turbulent flow and a larger effect at high Reynolds numbers than at low. At a Reynolds number of 10^6 and $u_\infty/\nu_\infty = 4.48 \times 10^5$ per inch, there is an 8-percent heat leakage for laminar flow and a 6-percent leakage for turbulent. At lower unit Reynolds numbers this error increases rapidly until, at $u_\infty/\nu_\infty = 1.52 \times 10^5$ per inch, the ratio is 18 percent for laminar and 14 percent for turbulent flow at $Re_x = 10^6$. The large magnitudes of the latter conduction errors preclude the usefulness of the heat-transfer results obtained at low unit Reynolds numbers.

The error caused by the radial heat conduction in the equilibrium results also has been computed but has been found to be very small. The magnitude of the error is only $+1^\circ$ F for an average test condition, or +0.2 percent of the true temperature.

There is an apparent limitation in the application of the preceding analysis. The calculations assume that transition from laminar to turbulent flow occurs at the same x location inside and outside the cylinder model. If the external flow had an extremely large transition Reynolds number whereas the internal flow was only moderately stable, the conduction correction would become somewhat larger than the values given in figure 19. For the rather extreme case of $h_1/h_2 \approx 0.1$ with $u_\infty/\nu_\infty = 4.48 \times 10^5$ per inch and $Re_x = 10^7$, the value of q_{corr}/q_{meas} would go from 0.81 to 0.77, which is not a very substantial increase in conduction error. It will therefore be assumed that the corrections indicated in figure 19 are satisfactory under widely varying flow conditions. It should be recalled that because of the steady-state assumptions they are still conservative and that the true heat leakage may be even less than the values given.

Correction for Nonisothermal Wall Temperature

Implicit in the calculation of the theoretical heat-transfer coefficients is the assumption that the wall is at a uniform temperature at each instant of time. That this is not the case is evident from the experimental temperature distributions shown in figure 18, where only that part of the temperature distribution having the largest nonuniformities is shown. A calculation of the effect of a nonuniform surface temperature on the heat transferred based on the method of reference 10 has been made for the temperature distributions given in figure 18, assuming

laminar flow. The results of the calculations are given in figure 20 and are expressed in terms of $St_{nonisothermal}/St_{isothermal}$. These results are to be interpreted as a multiplicative correction for the theoretical laminar curves presented in figures 11 to 13, or as divisors for correction of the experimental data points. Figure 20 indicates values of the Stanton number ratio as high as 2.5 near the leading edge, dropping to an average value of about 1.1 at distances more than 6 inches from the leading edge.

The preceding corrections are representative of the laminar boundary layer only. Similar calculations made on all turbulent boundary layers indicate smaller corrections. Definite corrections in the transition region cannot be made, since heat-transfer coefficients and boundary-layer characteristics are not known; however, the absence of large temperature variations in the transition region, compared with the leading-edge region, and the feeling that transitional heat-transfer coefficients are large suggest smaller corrections.

There is also some question regarding the nonuniform temperature correction in the equilibrium case, particularly in the transition region where a substantial temperature peak occurs. Because the heat transfer in the transition region and the actual mechanism of transition have not been established, it is difficult to say what role nonuniform temperatures play in the equilibrium temperature distribution.

Radiation Errors

A calculation of the radiation errors in the equilibrium and transient cases has been made for the cylinder with a laminar boundary layer. Assuming that heat is radiated from the tunnel walls, which are at the turbulent recovery temperature, and from the inner cylinder, also assumed conservatively to be at the turbulent recovery temperature, a correction to the measured recovery temperature on the test plate was computed. This correction amounted to $+1/2^{\circ}$ F at $u_{\infty}/\nu_{\infty} = 4.5 \times 10^5$ per inch and $+2^{\circ}$ F at $u_{\infty}/\nu_{\infty} = 1.5 \times 10^5$ per inch. These corrections when expressed in terms of recovery factor give errors of 0.1 and 0.3 percent.

Likewise, radiation correction calculations to the laminar heat-transfer rate were also made. Assuming that both the tunnel wall and inner cylinder are radiating at their turbulent recovery temperatures, calculations show that the measured conductive heat-transfer rates are about 3 percent high at the lowest unit Reynolds number. At the higher unit Reynolds number this figure drops to 1 percent.

Summary of Errors

The following data summarize the pertinent errors in the experimental points for the equilibrium and transient test conditions. The errors for the transient conditions must be subtracted from the experimental points shown in figures 11 to 14.

Equilibrium conditions. -

Wall total-temperature instrumentation and calculation error of $\pm 0.5^{\circ}$ F or, in percent,	± 0.1
Wall temperature error due to axial heat conduction in laminar region, percent	$+2.0$
(In the turbulent region the error is expected to be $<<2$ percent, but in the transition region it is not known)	
Wall temperature error due to radial heat conduction in laminar region, percent	$+0.2$
(This error should be less in the transition and turbulent region)	
Wall temperature error due to radiation $<2^{\circ}$ F or, in percent,	$+0.3$
Estimated total error in equilibrium temperature in Laminar region, percent	[a] $+2.5$
Turbulent region, percent	[a] $<+0.5$

Transient conditions. -

Total-temperature error due to instrumentation and method of calculation, $^{\circ}$F	± 0.5
Wall temperature error due to instrumentation and method of calculation, $^{\circ}$F	± 2.0
Temperature-time slope error, percent	± 3.0
Error in heat transfer due to assumption $T_{aw} = 0.9\ T_0$, percent	± 5.0
Error caused by variation in test-surface thickness, percent	± 3.0
Axial heat-conduction error in laminar region, t = 14 seconds at $x \geq 2$ inches, percent	$+1.0$
(Negligible error in turbulent region)	
Radial heat-conduction error at $u_\infty/\nu_\infty \approx 4.5 \times 10^5$/in., $Re_x = 10^6$, percent	$+8.0$
$u_\infty/\nu_\infty \approx 1.5 \times 10^5$/in., $Re_x = 10^6$, percent	$+18.0$
Error in heat-transfer coefficient for nonisothermal wall condition $x > 6$ inches, laminar region, t = 14 sec, percent	$+10.0$
Heat-transfer radiation error at $u_\infty/\nu_\infty = 4.5 \times 10^5$/in., percent	$+1.0$
$u_\infty/\nu_\infty = 1.5 \times 10^5$/in., percent	$+3.0$

[a]The estimated total errors in temperature correspond to errors of 3 percent and 0.6 percent in the recovery factor.

Estimated total error in heat-transfer coefficient in
Laminar region at $u_\infty/\nu_\infty = 4.5\times10^5$/in., percent . . . . . 20±6
Turbulent region at 4.5×10^5/in., percent . . . . . 9±6
Laminar region at $u_\infty/\nu_\infty = 1.5\times10^5$/in., percent . . . . . 32±6
Turbulent region at 1.5×10^5/in., percent . . . . . 21±6

The preceding data indicate that the equilibrium results have small errors (0.5 to 2.5 percent) in both the laminar and turbulent region, whereas the heat-transfer results have acceptable accuracies only in the high unit Reynolds number, turbulent regions.

REFERENCES

1. Brinich, Paul F.: Effect of Leading-Edge Geometry on Boundary-Layer Transition at Mach 3.1. NACA TN 3659, 1956.

2. Moeckel, W. E.: Some Effects of Bluntness on Boundary-Layer Transition and Heat Transfer at Supersonic Speeds. NACA Rep. 1312, 1957. (Supersedes NACA TN 3653.)

3. Brinich, Paul F., and Sands, Norman: Effect of Bluntness on Transition for a Cone and a Hollow Cylinder at Mach 3.1. NACA TN 3979, 1957.

4. Diaconis, N. S., Jack, John R., and Wisniewski, Richard J.: Boundary-Layer Transition at Mach 3.12 as Affected by Cooling and Nose Blunting. NACA TN 3928, 1957.

5. Brinich, Paul F.: A Study of Boundary-Layer Transition and Surface Temperature Distributions at Mach 3.12. NACA TN 3509, 1955.

6. Chapman, Dean R., and Rubesin, Morris W.: Temperature and Velocity Profiles in the Compressible Laminar Boundary Layer with Arbitrary Distribution of Surface Temperature. Jour. Aero Sci., vol. 16, no. 9, Sept. 1949, pp. 547-565.

7. Jack, John R.: Effect of Favorable Pressure Gradients on Transition for Several Bodies of Revolution at Mach 3.12. NACA TN 4313, 1958.

8. Van Driest, E. R.: Turbulent Boundary Layer Flow in Compressible Fluids. Jour. Aero Sci., vol. 18, no. 3, Mar. 1951, pp. 145-160.

9. Jack, John R., Wisniewski, Richard J., and Diaconis, N. S.: Effects of Extreme Surface Cooling on Boundary-Layer Transition. NACA TN 4094, 1957.

10. Hartnett, J. P., Eckert, E. R. G., Birkebak, Roland, and Sampson, R. L.: Simplified Procedures for the Calculation of Heat Transfer to Surfaces with Nonuniform Temperatures. TR 56-373, WADC, Dec. 1956.

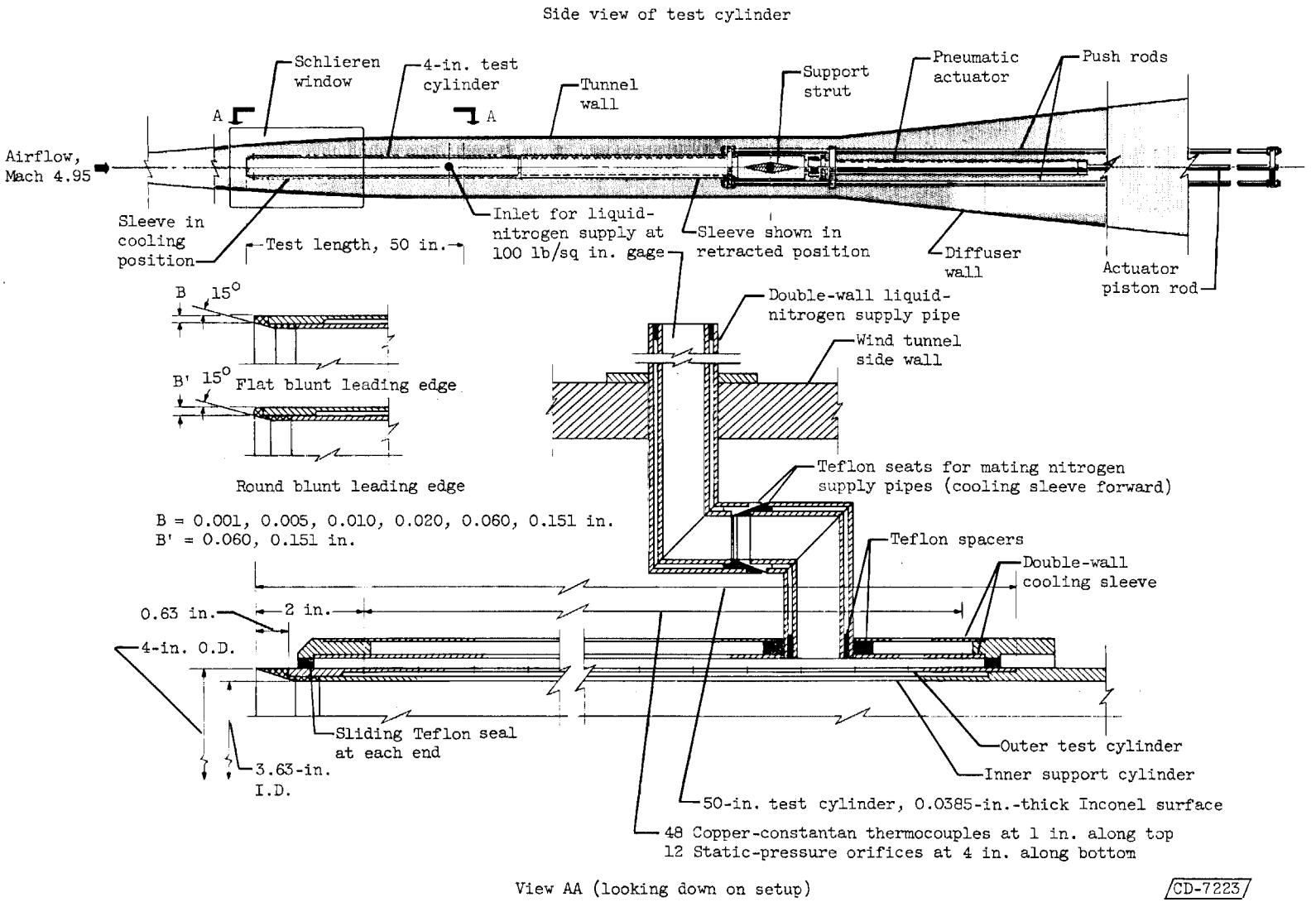

Figure 1. - Cylinder model, 4 by 50 inches, with cooling apparatus in 1- by 1-foot Mach 5 variable-Reynolds-number wind tunnel.

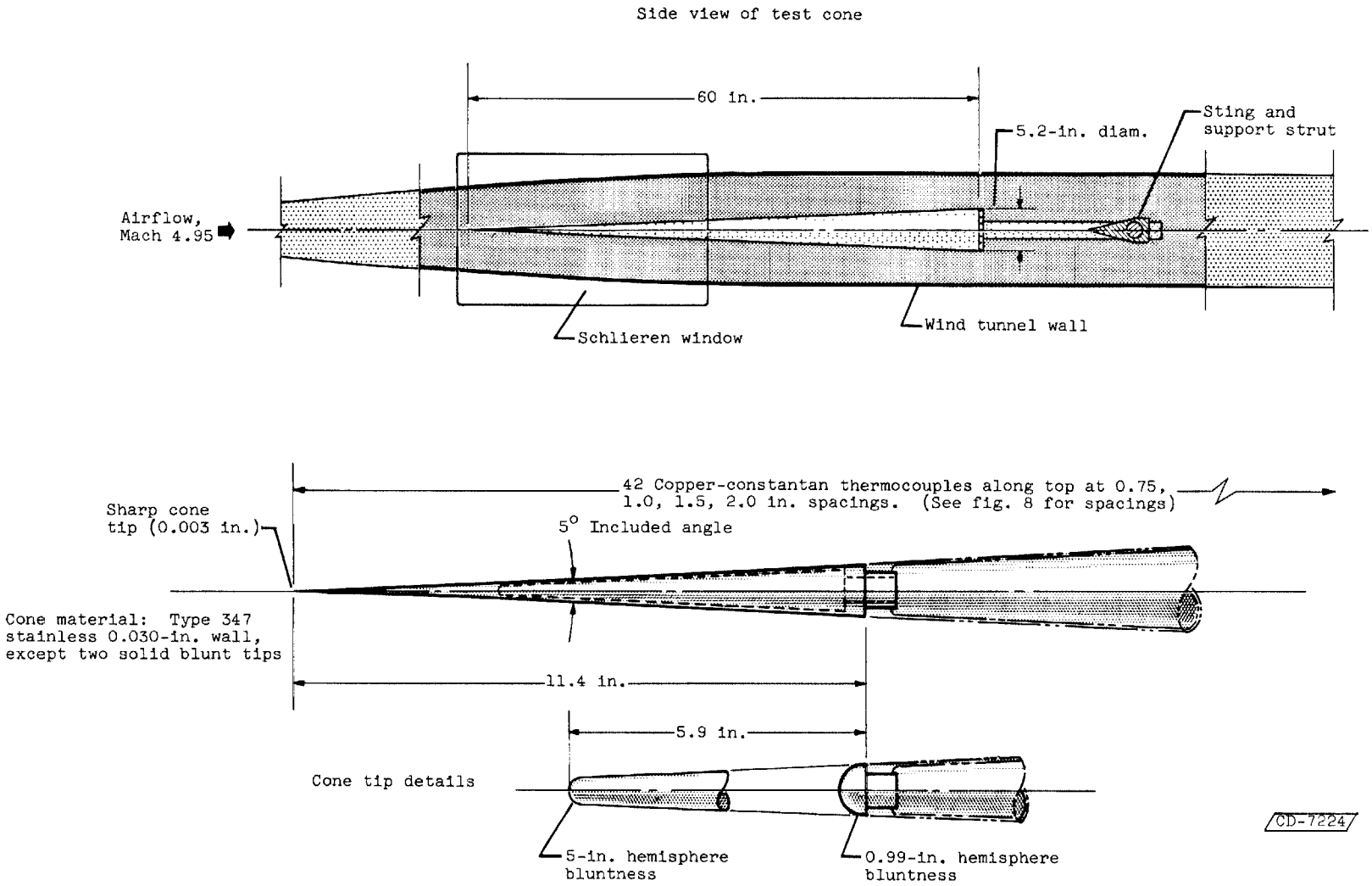

Figure 2. - Cone model, 5° by 60 inches, in 1- by 1-foot Mach 5 variable-Reynolds-number wind tunnel.

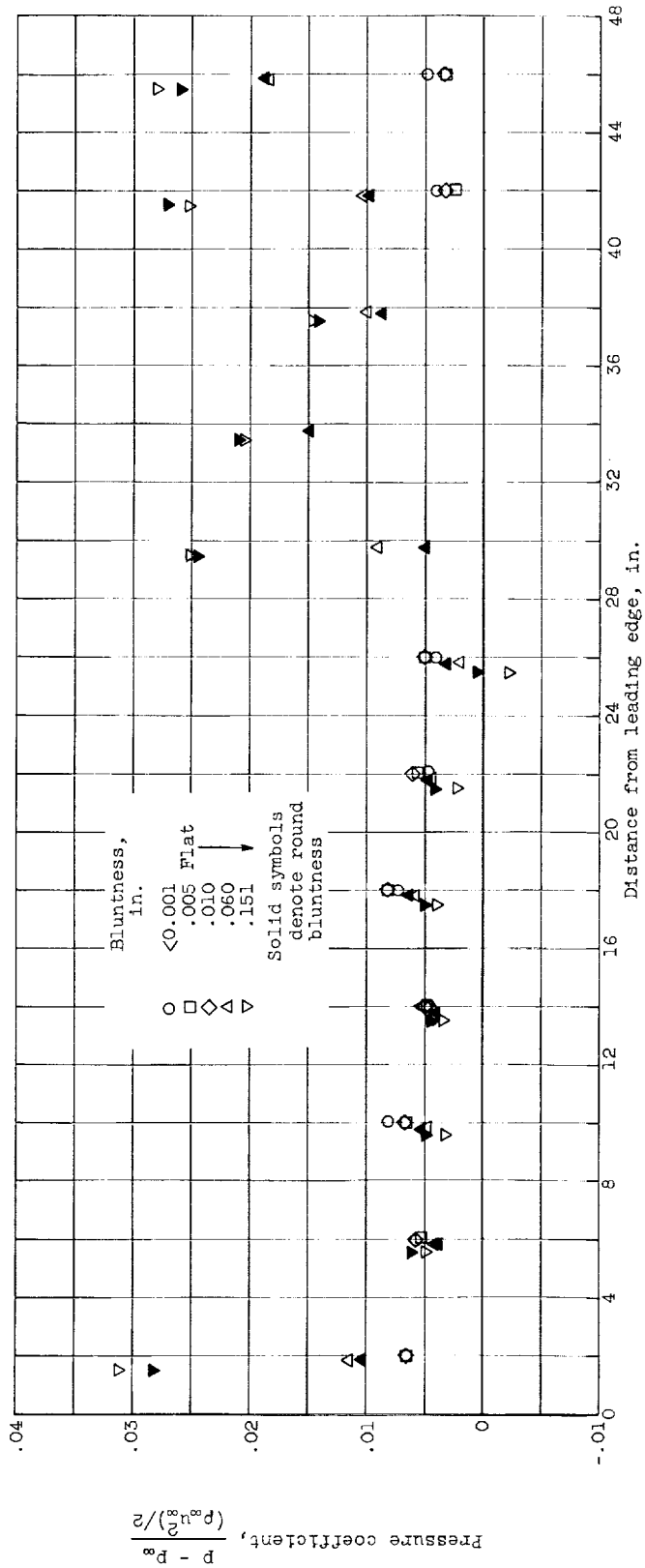

Figure 3. - Pressure distribution along cylinder model; $u_\infty/\nu_\infty = 4.5 \times 10^5/\text{in.}$

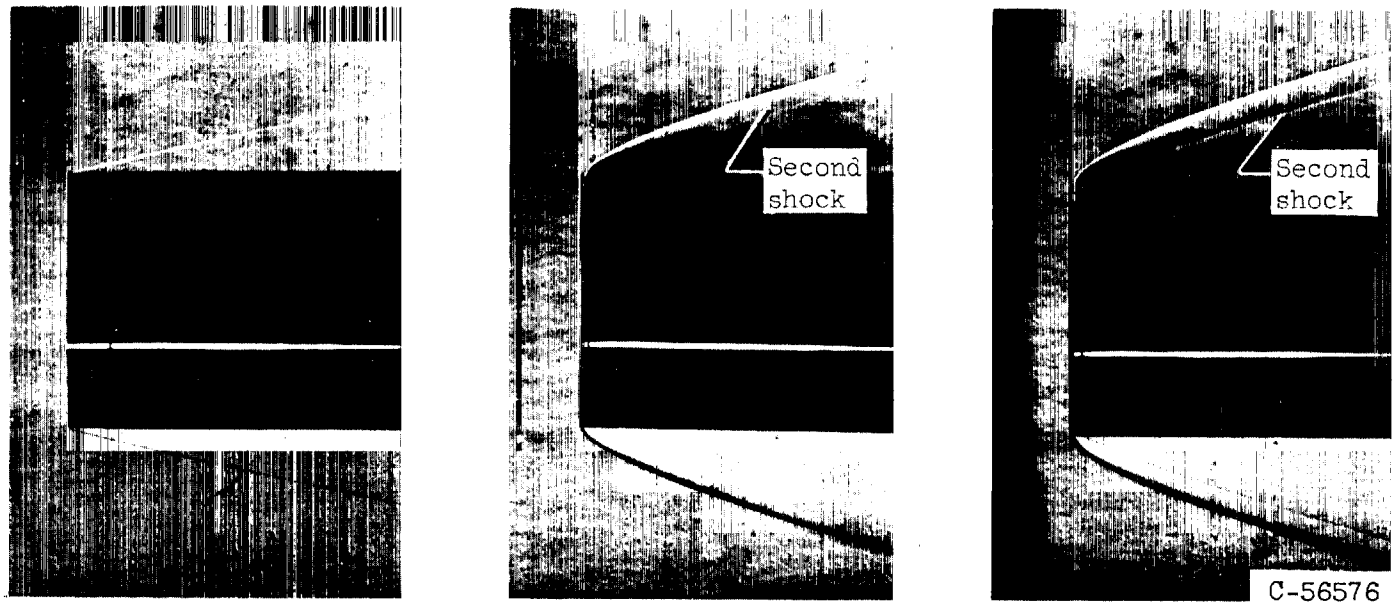

(a) Sharp leading edge.

(b) 0.151-inch round bluntness.

(c) 0.151-inch flat bluntness.

Figure 4. - Schlieren photographs illustrating secondary shock formation when leading edge of cylinder is blunted.

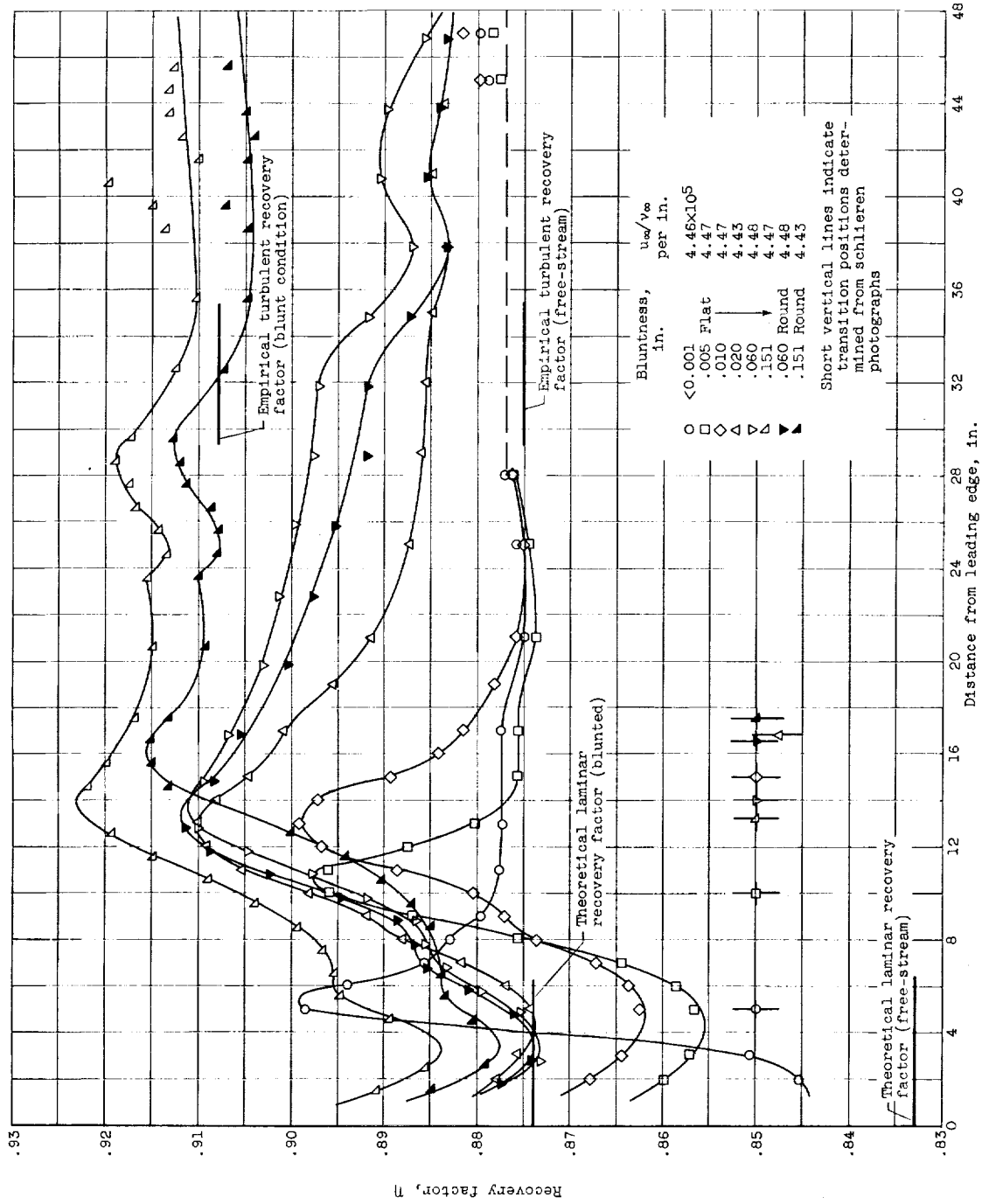

Figure 5. - Effect of bluntness on recovery factor distribution along cylinder model; $u_\infty/\nu_\infty \approx 4.5\times10^5$/in.

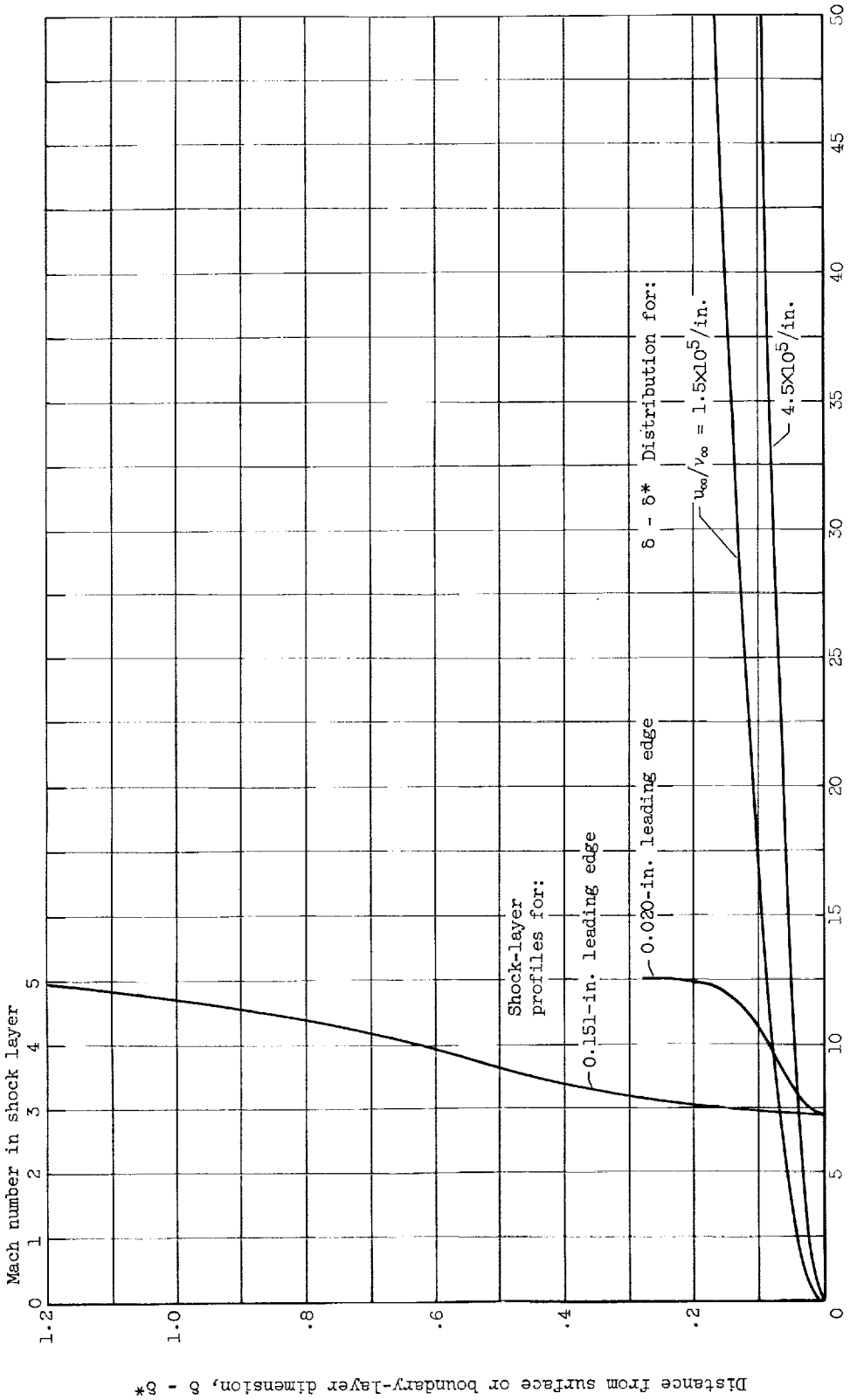

Figure 6. - Comparison of boundary-layer and shock-layer thicknesses on cylinder.

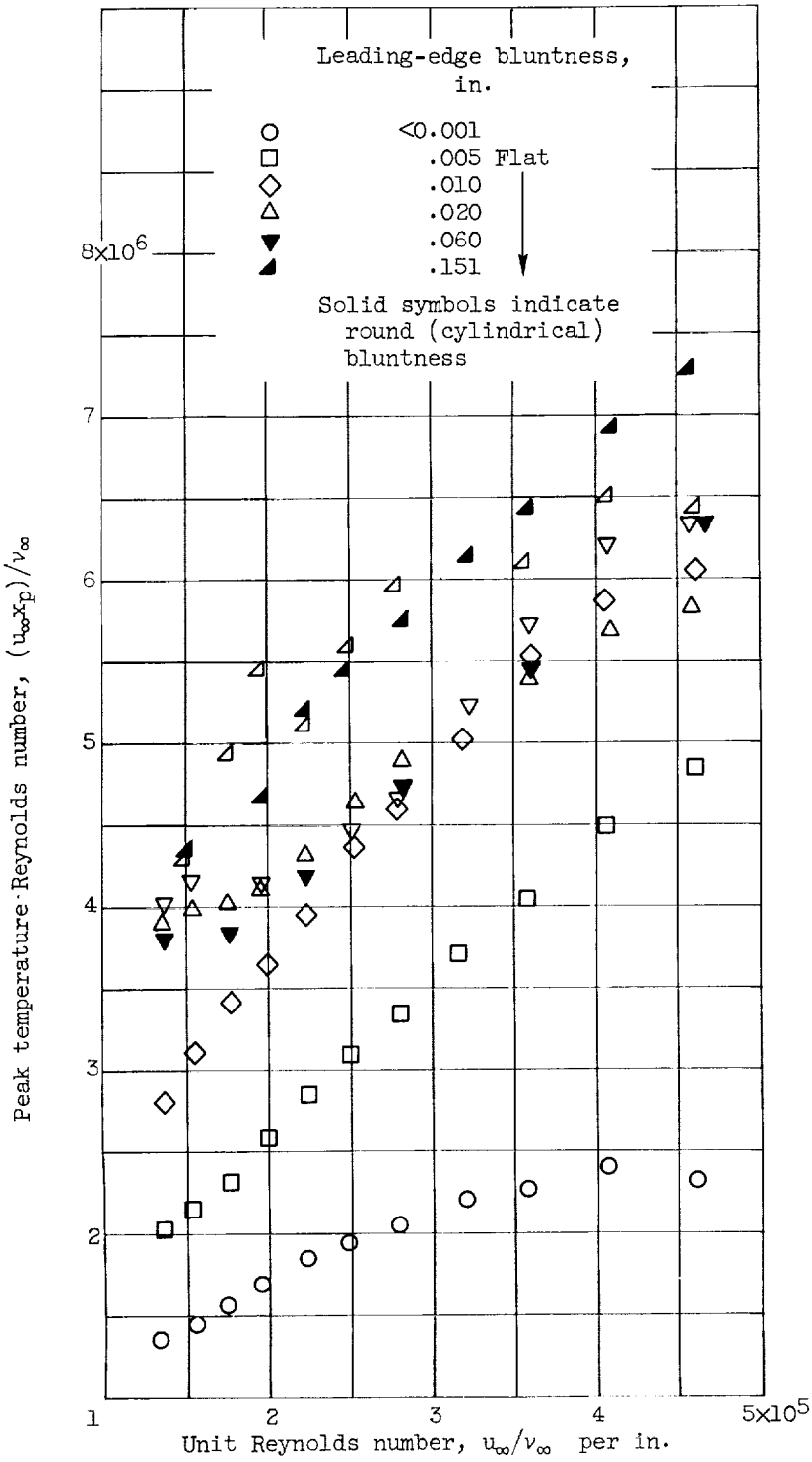

Figure 7. - Equilibrium peak temperature location on cylinder as function of unit Reynolds number and leading-edge bluntness.

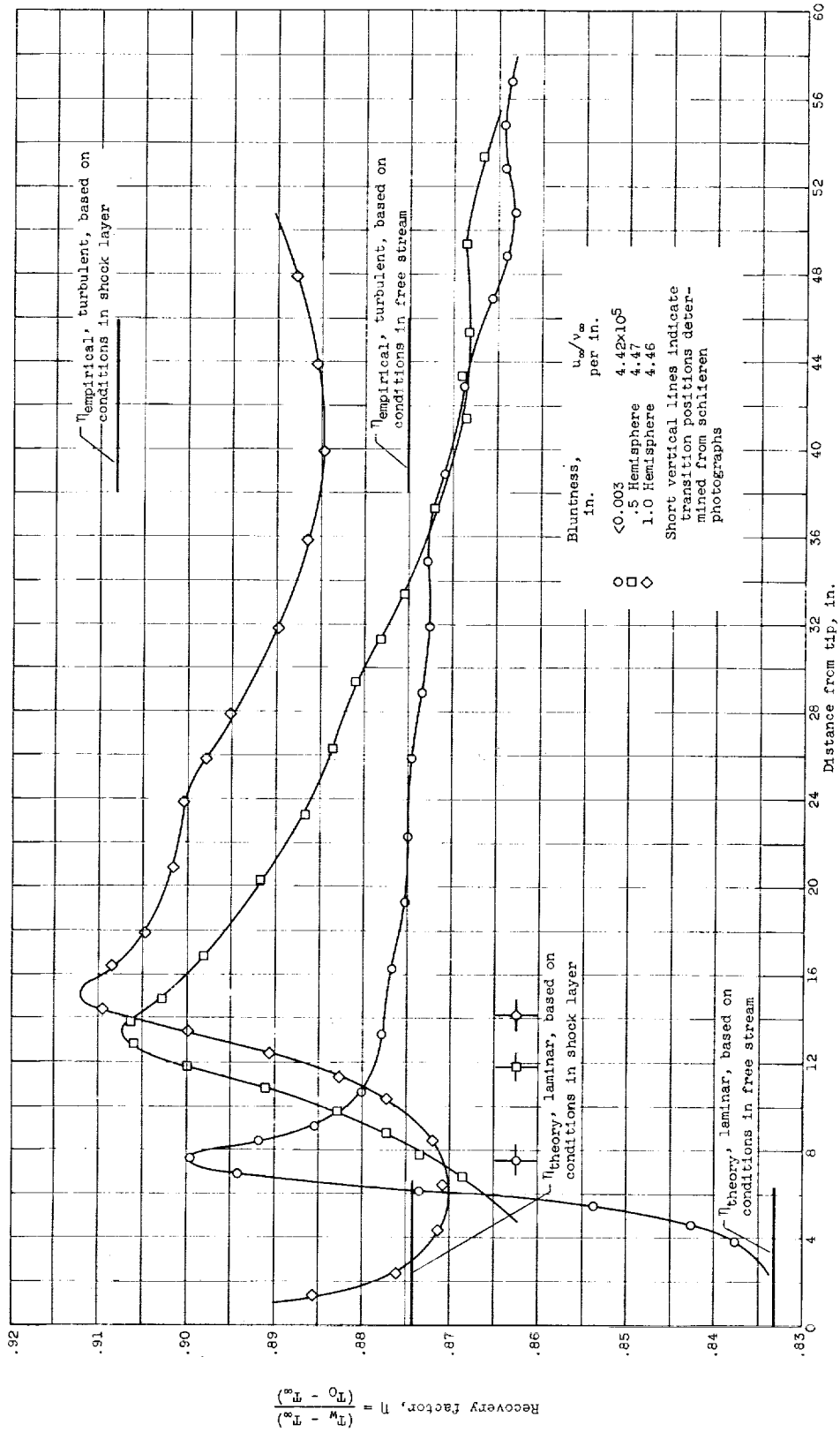

Figure 8. - Effect of bluntness on recovery factor distribution along cone model; $u_\infty/\nu_\infty \approx 4.5 \times 10^5$/in.

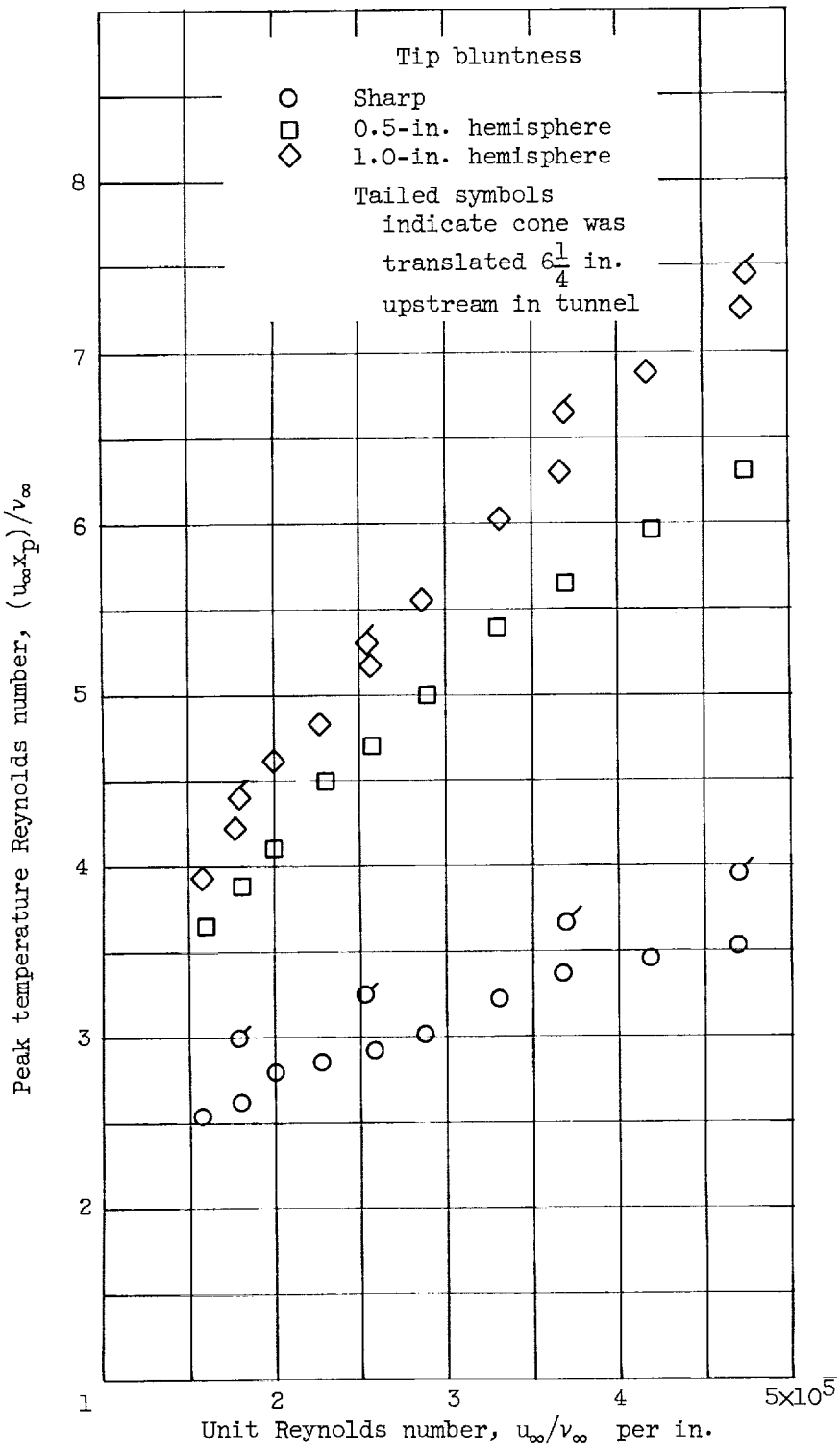

Figure 9. - Equilibrium peak temperature location on cone as function of unit Reynolds number and tip bluntness.

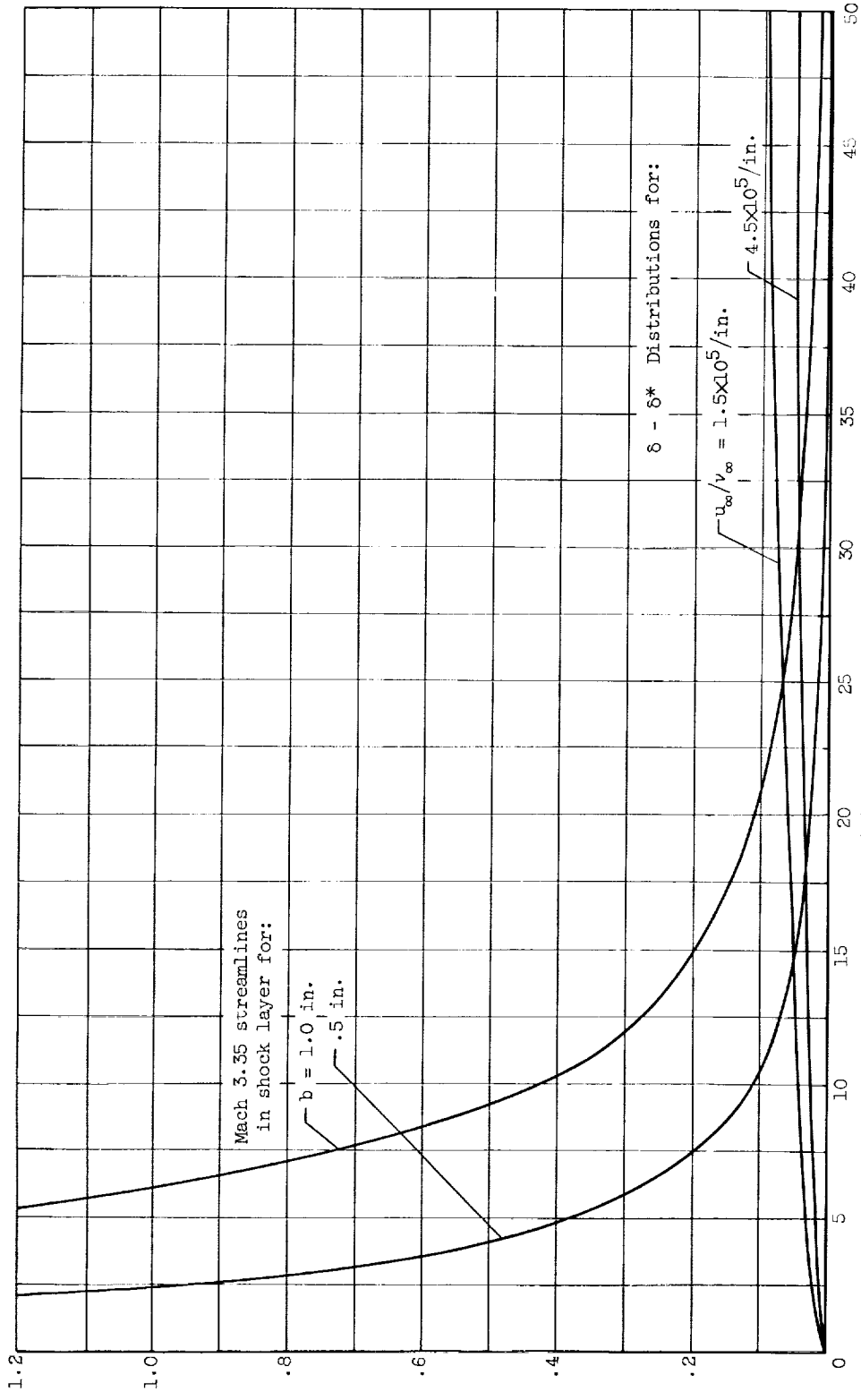

Figure 10. - Comparison of boundary-layer and shock-layer thicknesses on cone.

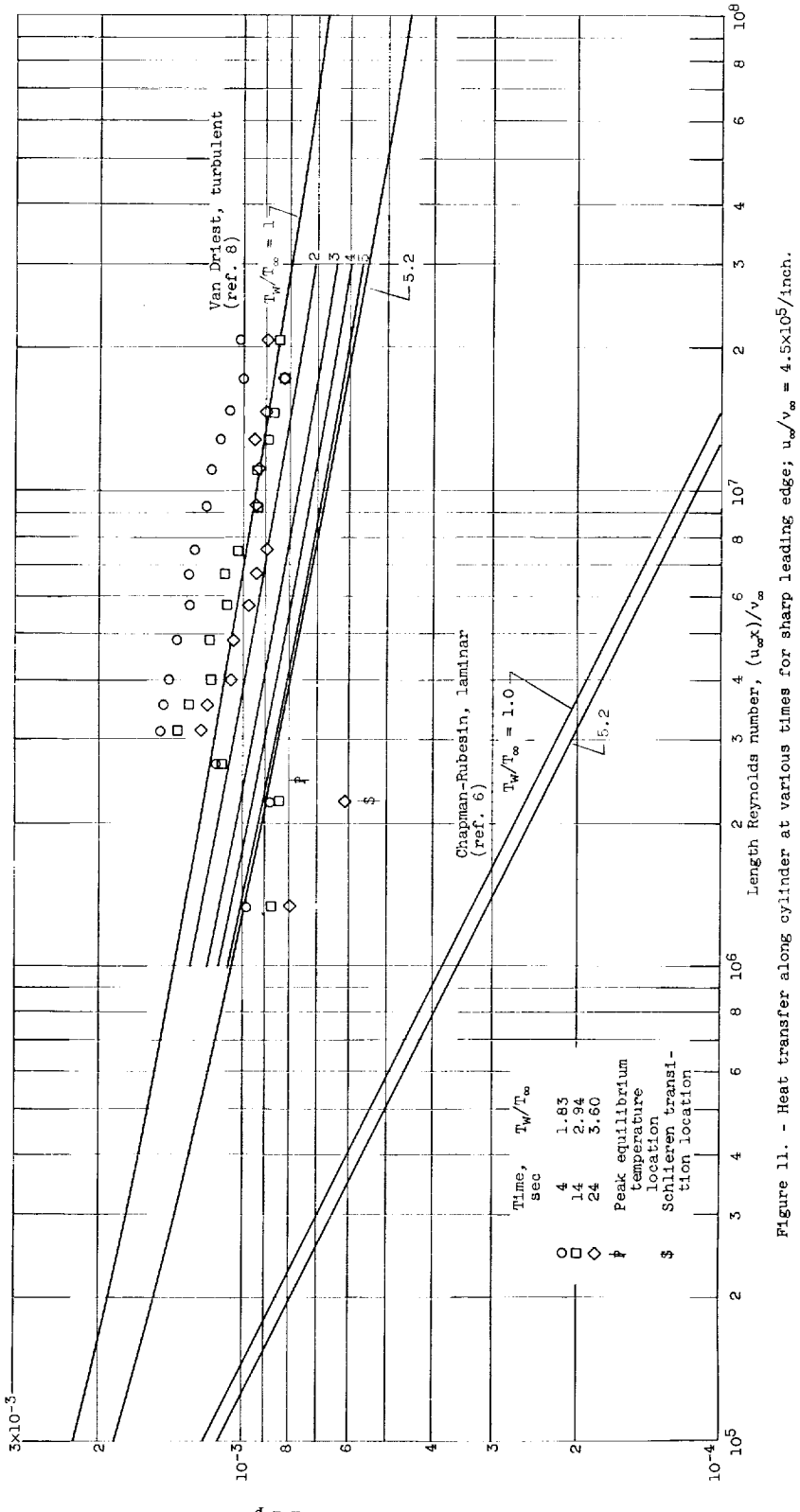

Figure 11. - Heat transfer along cylinder at various times for sharp leading edge; $u_\infty/\nu_\infty = 4.5 \times 10^5$/inch.

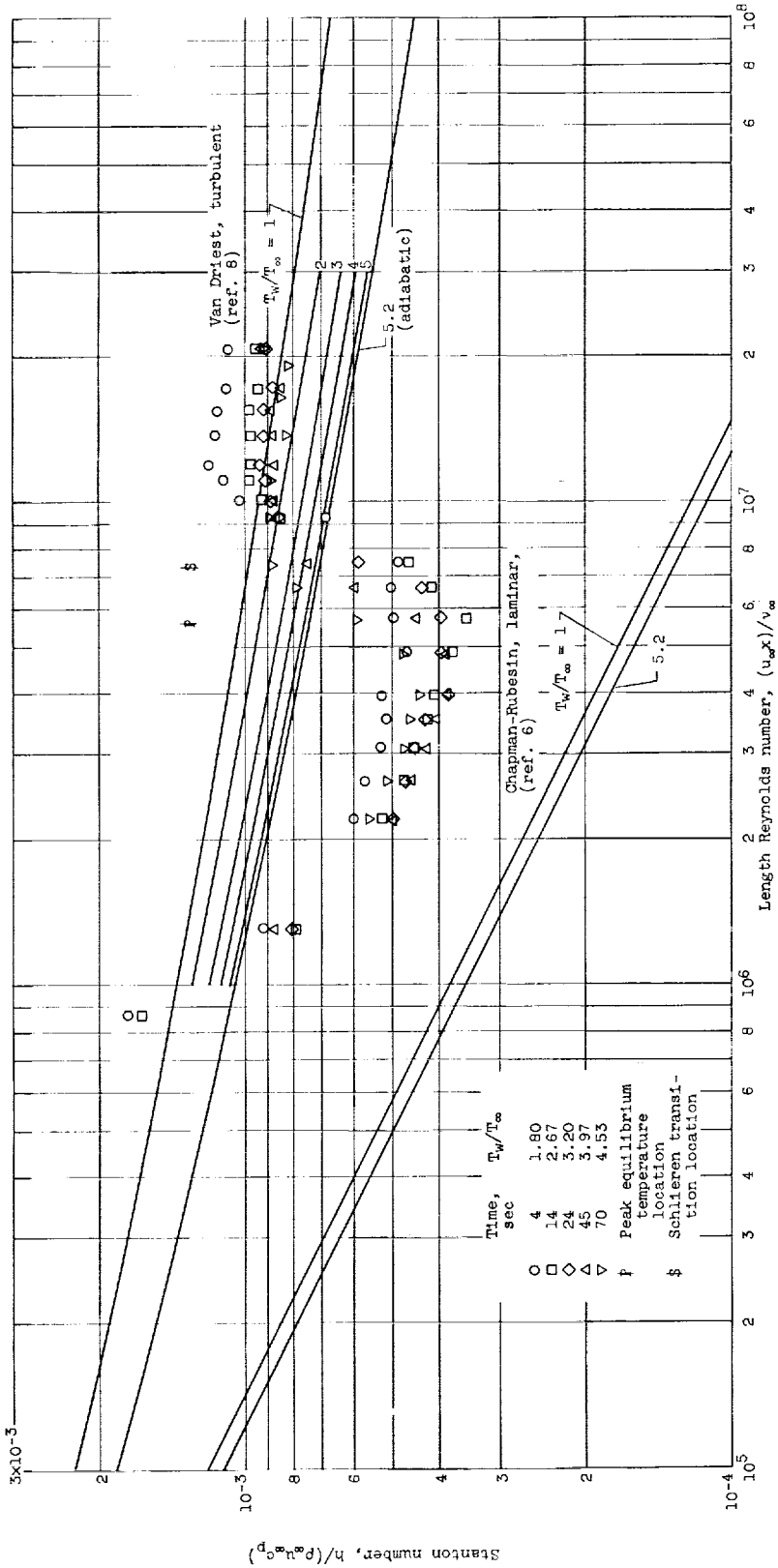

Figure 12. - Heat transfer along cylinder at various times for 0.020-inch leading edge; $u_\infty/\nu_\infty = 4.5 \times 10^5$/inch.

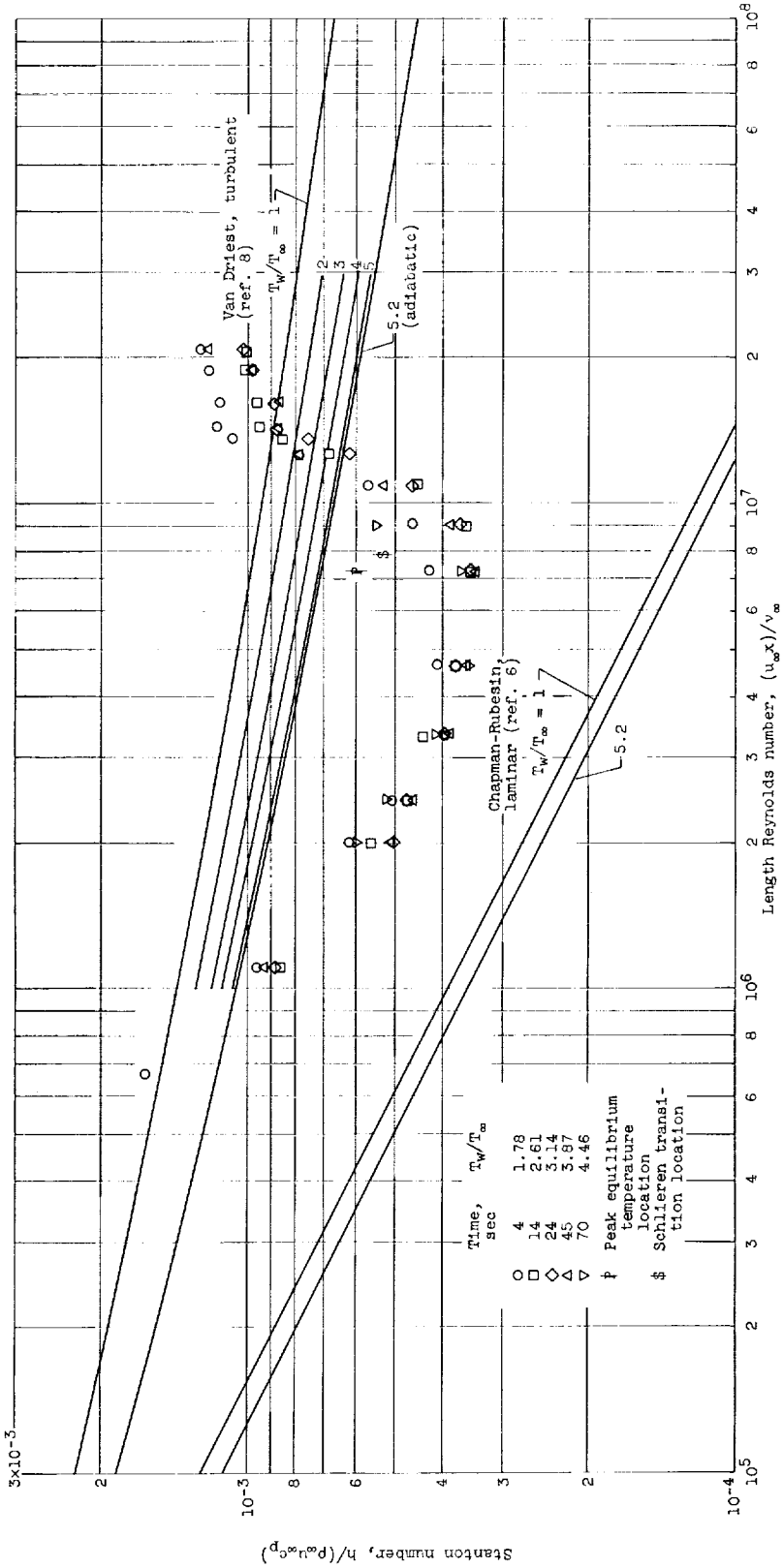

Figure 13. - Heat transfer along cylinder at various times for 0.151-inch leading edge; $u_\infty/\nu_\infty = 4.5 \times 10^5$/inch.

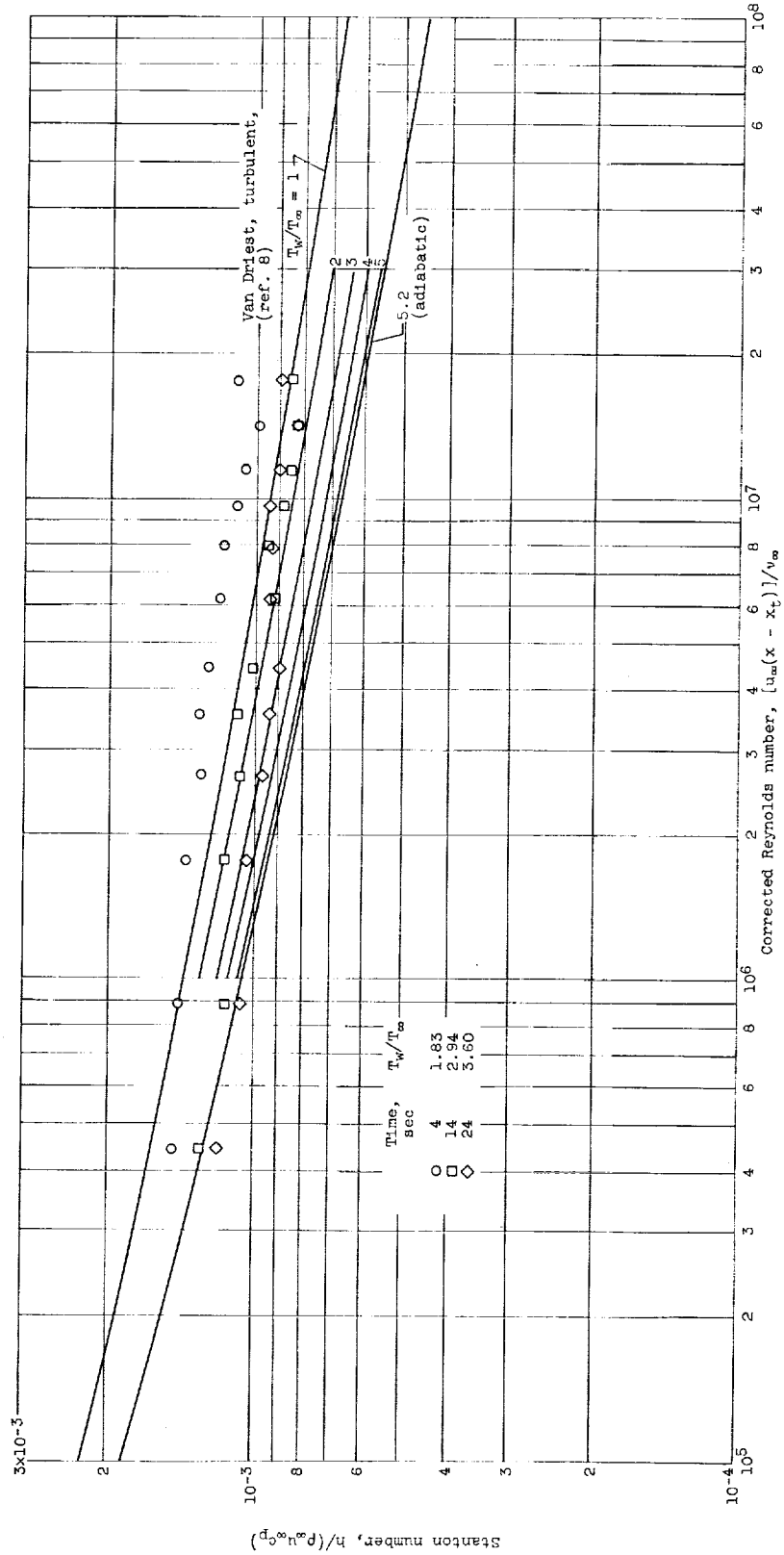

Figure 14. - Turbulent heat transfer along cylinder at various times with origin at transition point for sharp leading edge; u_∞/ν_∞ = 4.48x10^5/inch.

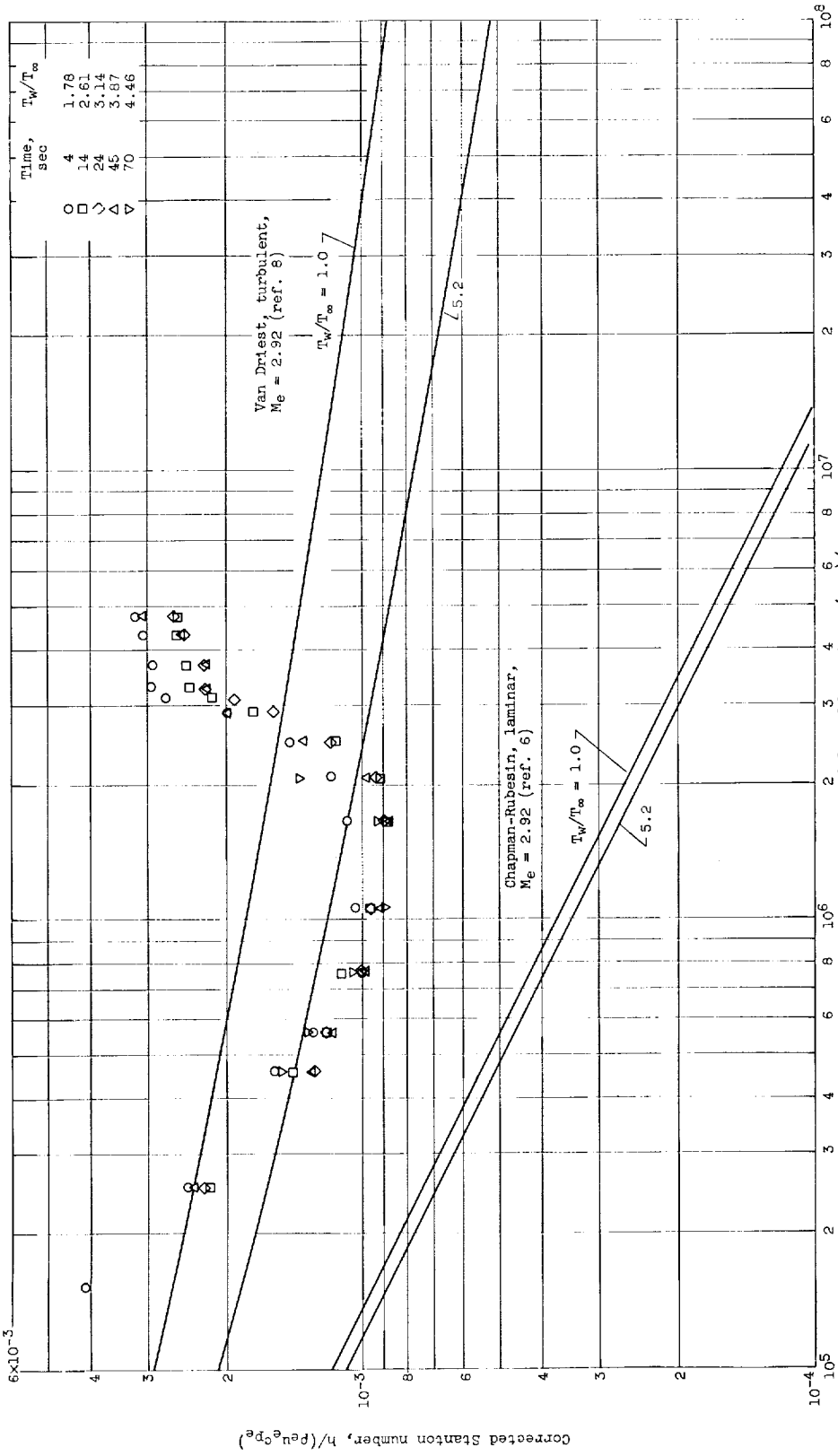

Figure 15. - Heat transfer along cylinder at various times based on shock-layer properties for 0.151-inch leading edge; $u_\infty/\nu_\infty = 4.5 \times 10^5$/inch.

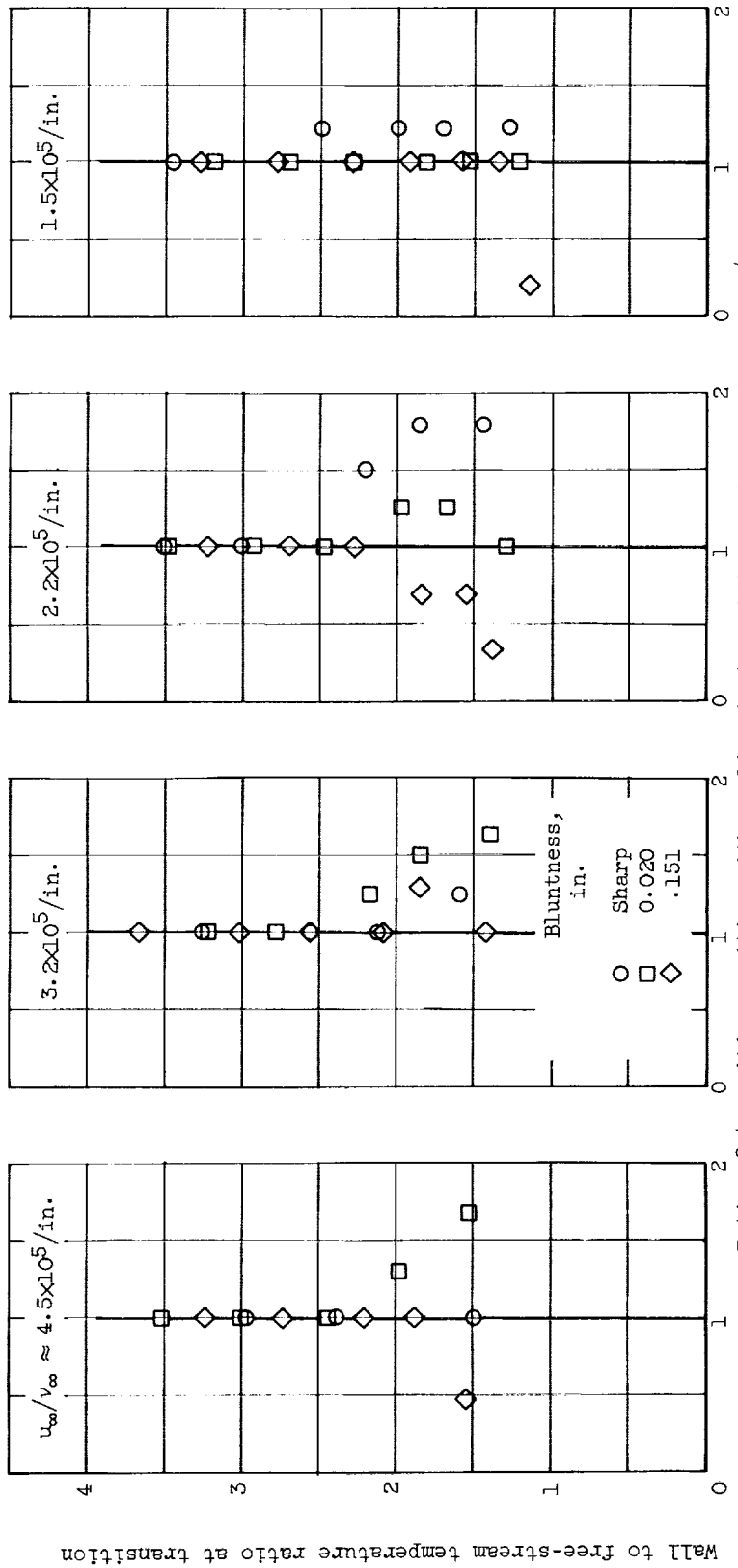

Figure 16. - Transition position as a function of wall temperature and bluntness on cylinder.

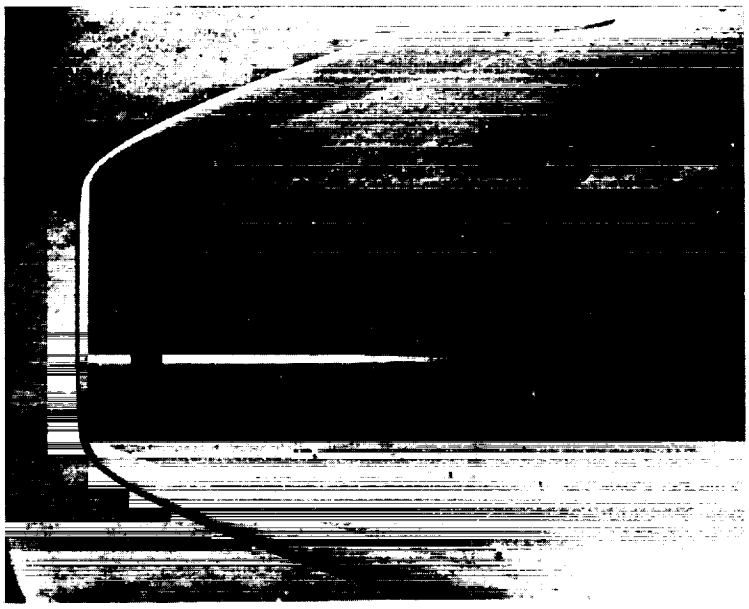

(a) Initial shock position.

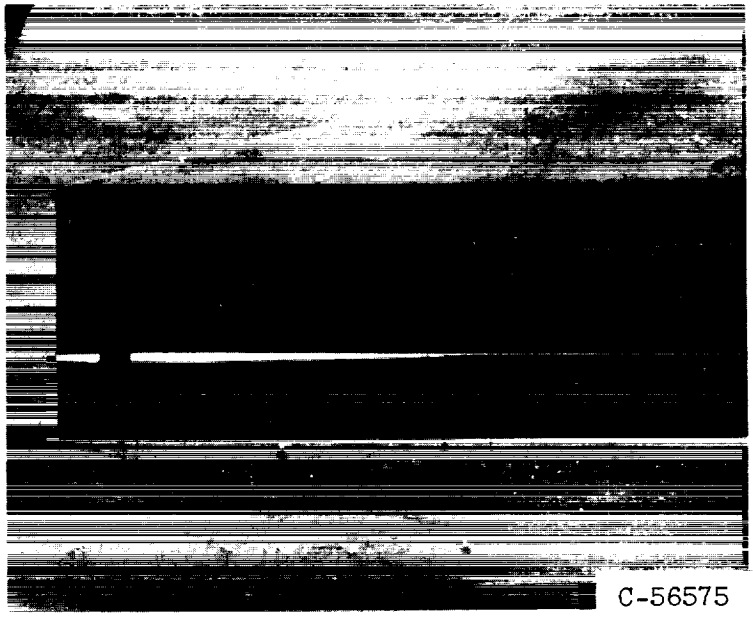

(b) Shock position after cooling sleeve was fully retracted.

Figure 17. - Schlieren photographs illustrating leading-edge shock configuration for sharp leading edge of cylinder; u_∞/ν_∞ = 1.96x 10^5/inch.

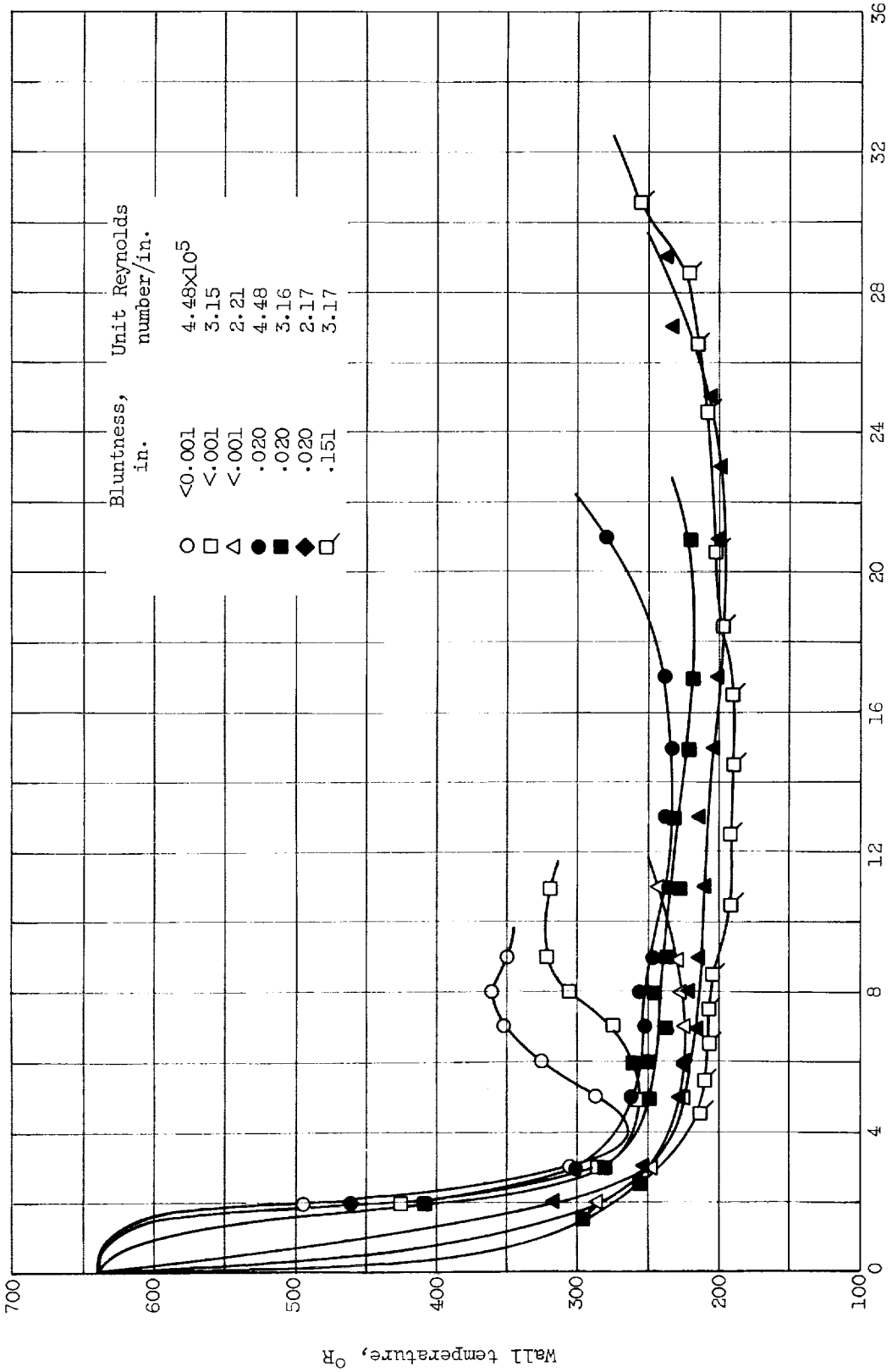

Figure 18. - Wall temperature distributions along cylinder at time t = 14 seconds.

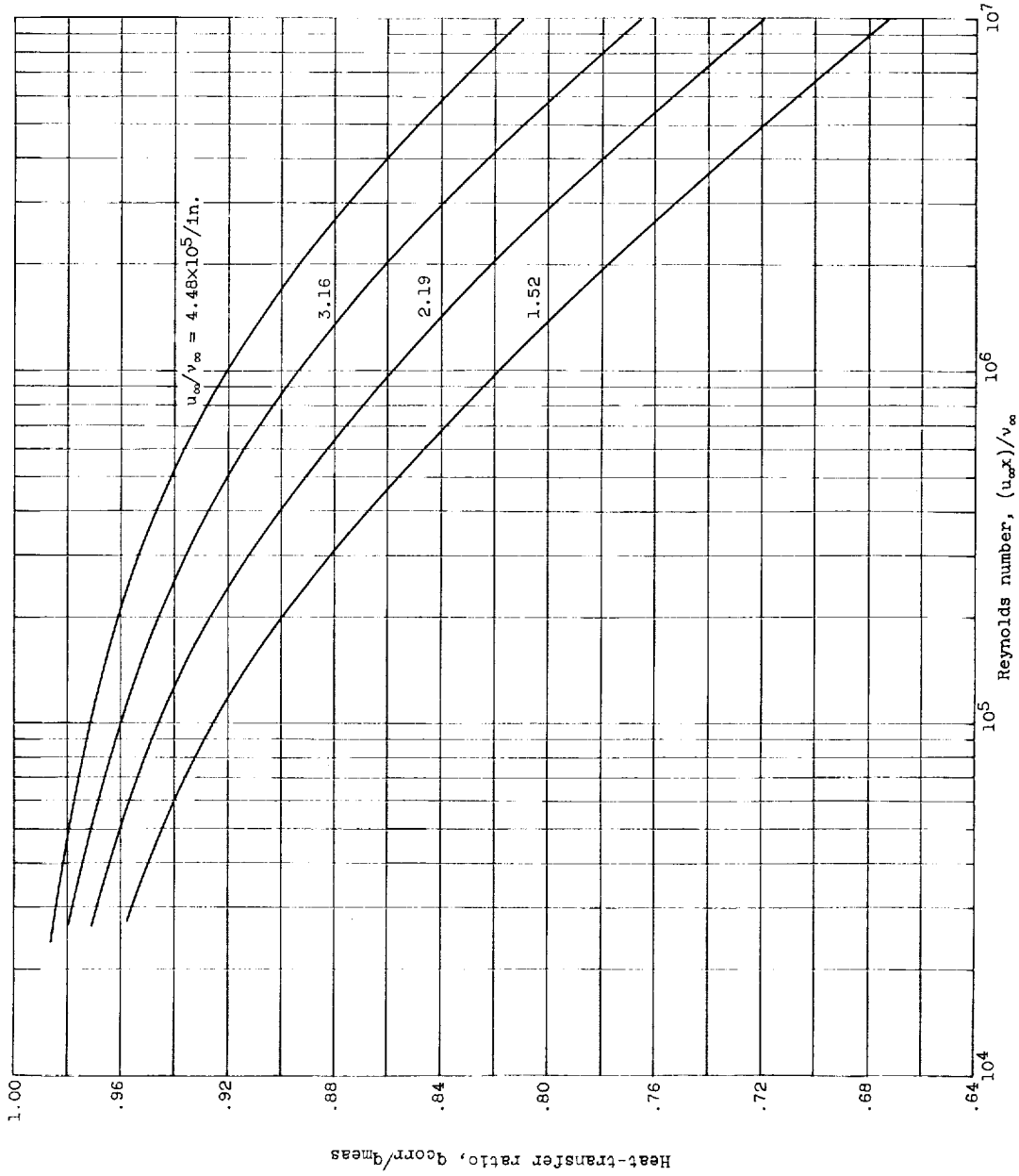

(a) Laminar flow.

Figure 19. - Heat-transfer correction for radial heat conduction on cylinder model; $T_w/T_\infty \approx 1$.

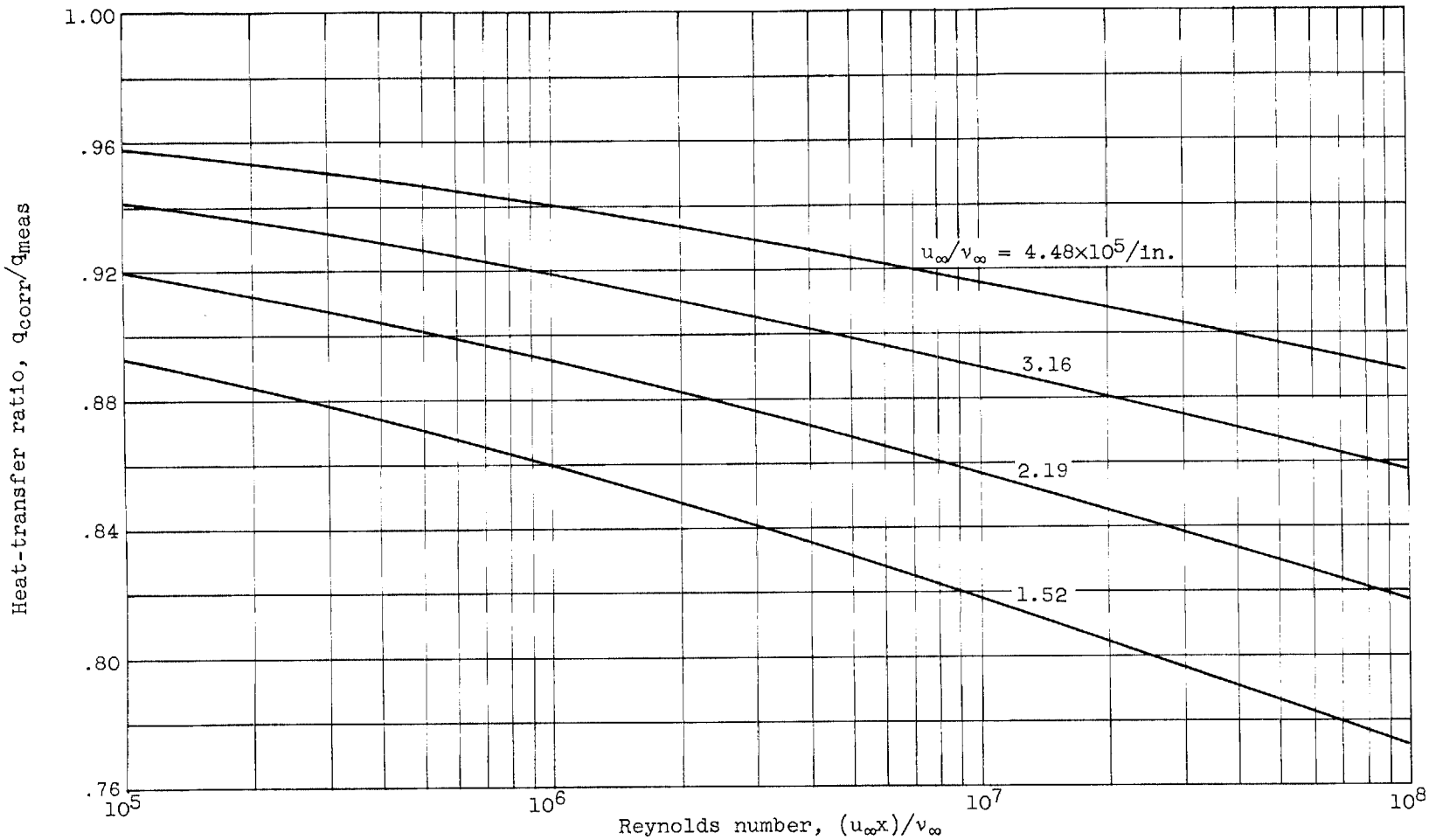

(b) Turbulent flow.

Figure 19. - Concluded. Heat-transfer correction for radial heat conduction on cylinder model; $T_w/T_\infty \approx 1$.

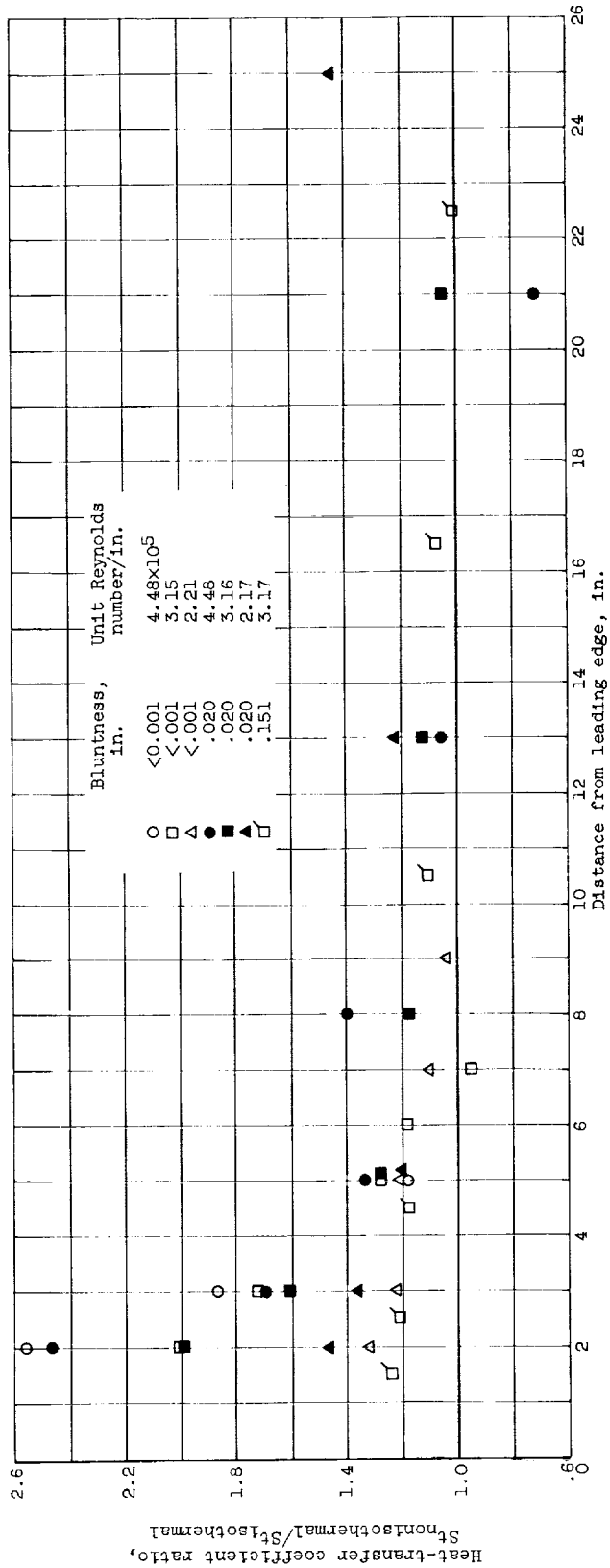

Figure 20. - Effect of nonisothermal wall condition of cylinder on laminar heat-transfer coefficient.